nature portfolio

Peer Review File

Unveiling Mechanisms and Onset Threshold of Humping in High-Speed Laser Welding

Corresponding Author: Professor Jingjing Li

This file contains all reviewer reports in order by version, followed by all author rebuttals in order by version.

Version 0:

Reviewer comments:

Reviewer #1

(Remarks to the Author)
This paper explores the fascinating topic of utilizing X-ray synchrotron imaging to observe the flow of melt pools and the evolution of defects. The authors employ a combination of experimental X-ray techniques and simulations to validate and investigate various phenomena. The paper appears to be quite impressive. However, I wonder why the authors chose to use very thin metal sheets. Is this study purely academic or does it have practical applications? In real-world scenarios, weld thickness is often much greater, making it challenging to directly apply the findings and insights gleaned from this paper.

In the introduction, it would be beneficial to highlight potential applications for the investigation of ultra-thin sheets. For instance, ultra-thin sheets find relevance in various industries such as the manufacturing of lead frames for semiconductors, radiators for automotive applications, lithium batteries for electric vehicles, as well as in motors and stators. These applications signify the importance of understanding the behavior of ultra-thin sheets, as highlighted in research studies such as those mentioned in the link provided.
While I don't require you to cite this paper, it's evident that this paper represents one of the few instances discussing applications of extremely thin sheets for welding.
https://www.sciencedirect.com/science/article/pii/S1526612522004261
If due to the limitations of X-ray photon sources, I recommend considering conducting this type of experiment at the ESRF in France. They possess significantly higher power capabilities, enabling experimentation with thicker plates.

On the other hand, let's delve into the humping phenomenon using X-ray or high-speed camera techniques for welding. Despite the abundance of literature on welding, joining, and additive manufacturing with similar mechanisms, exemplified by papers from Dr. Nguyen Van Anh (https://www.sciencedirect.com/science/article/pii/S1526612520306885) or Prof. ChuanSong Wu on plasma arc welding, the phenomena discussed in your paper are not groundbreaking. The mechanisms you address are well-known. However, the novelty in your research lies in its application to very ultra-thin sheets. Additionally, you've conducted supplementary simulations to provide evidence and validation, distinguishing your work from existing studies.

Regarding the velocity claim of exceeding 6 m/s, it's crucial to provide more evidence or validation for this value. Is there sufficient data to support its accuracy?
Including a scale in Figures 2 and 3 would greatly enhance clarity and aid in interpretation.

Could you please elaborate on the welding process used for joining the two plates? Specifically, did you utilize a butt-joint or an overlap joint? If an overlap joint was employed, please provide detailed information.
Additionally, it would be beneficial to provide more comprehensive details about the X-ray system, parameters, and experimental setup. Including images of the experimental setup could significantly improve understanding, particularly considering the challenges associated with working with very ultra-thin sheets and utilizing X-ray technology.
Given the difficulty of setting up experiments with ultra-thin sheets and the similarities with X-ray technology, discussing any novel insights or differences compared to results obtained with thicker materials would be valuable. Discuss these differences by cite other papers could make a substantial contribution to the fields of welding, joining, and additive manufacturing, particularly at the microscale thickness level, where most researchers focus on thicker materials.

Reviewer #2

(Remarks to the Author)
Their findings indicate that the short keyhole rear wall, the high backward melt velocity, and the prolonged tail of melting pool are the primary factors contributing to the onset of humping. Also, a dimensionless humping index was introduced in this study. There are some comments listed below:
(1) The data shown in Fig.1 (b) and (c) are so coherent. Reviewers also would like to see the comparisons between the simulation and experimental data in the average height of humpings.
(2) In your modeling, the surface or volumic heat source was used? It matters to your simulation results and please explain why you chose one of them.
(3) MW, what unknown parameters that you use for experimental fitting? Or you did not use the fitting way between simulation and experimental data? All need to be explained in detail.
(4) Please list a table to illustrate all the numbers that you set in those unknown parameters. Are those temperatures independent or dependent? For example, thermal conductivity, surface tension coefficient, recoil pressure.....
(5) Several papers have mentioned about the humping due to Rayleigh's instability. From the simulation results, you even add more explanations in humping, for example, the shorter keyhole rear wall, ..., however in your simulation, could you see the humping cycle? To me, the humping will happen all the time in your modeling, am I right? Just as you mentioned, the humping cycle was analyzed with several "instantaneous" MP characteristics. The observation aligned well with the humping theory based on the conservation of volume. Please explain it in detail.
(6) I just wonder if the no-humping zone is optimal in mechanical properties in bonding. Please confirm if the mechanical properties such as shear strength, porosity,..... in bonding are better. To me, the no-humping zone is only for those parameters without humping, but the qualities of the bonding still need to study furthermore.
(7) Finally, is it possible to use the hybrid manufacturing way to cool down the tail of melting pool at once to suppress humping? Please comment.
Those comments from above are mandatory in the revised manuscript. The quality of this submitted paper is worthy to be published.

Version 1:

Reviewer comments:

Reviewer #1

(Remarks to the Author)
Thank you for your effort in revising the manuscript. I have some additional questions and comments.
The humping phenomenon is significantly related to the velocity of fluid flow in the melt pool, the behavior of convection patterns, and the appearance of eddies. Discuss more details in quantity based on velocity change is must better. In addition. The humping phenomena is can also depend on the heat input used. Please include a table comparing the heat input in all cases to help discuss the phenomena.
However, I did not see a detailed discussion about the velocity of fluid flow, the behavior of convection patterns, and the appearance of eddies in the melt pool, especially velocity, in relation to your results. If you have calculated fluid flow velocity, please explain the methods, calibration, and steps used in detail. For guidance, you can refer to the paper: https://iopscience.iop.org/article/10.1088/1361-6463/aa9902/meta. For example, do you use zirconia particles to track the velocity change or any other method? How did you do with it because you did for very very thin sheets?
Maximal melt velocity of 6.0 m/s in Figure 2f needed to provide evidence?
You mentioned that calculating velocity by experiment is very challenging, and you selected the simulation approaches; it may be OK. But all papers you cited, ref 34, 35, 36, are calculating velocity based on X-rays or other experiments. Therefore, your argument lacks conviction. In addition, ref 35 uses only one X-ray to calculate velocity. Therefore, only 2D images of the melt pool can be revived, and I believe the results may be challenging.
Additionally, I don't understand why the humping phenomenon is primarily explained based on CFD results when you have X-ray video data. Discussing the phenomenon based on the X-ray video rather than simulations would be more reliable. You need to include more details based on velocity, convection pattern behavior, and/or the appearance of eddies.
In a recent paper, Anh et al. explained undercut and other defects in the Plasma keyhole welding process based on experiments: https://s3.amazonaws.com/WJ-www.aws.org/supplement/2019.98.018.pdf. You should read this as well. They based their explanations on X-ray images, velocity calculations, and convection patterns to explain the phenomena of undercut and other defects in detail and reliably.
Moreover, I am concerned about your use of only one X-ray source, resulting in 2D projected images of the melt pool, which seems insufficient for calculating the velocity. How do you address this issue? Additionally, the mechanism of humping formation is not clearly explained in the qualitative analysis.
Is your CFD model 2D or 3D? If it is a 3D model, it does not match your experiment, which provides only 2D melt pool images. If you are using CFD models to estimate the humping phenomenon, can you perform experiments under the same conditions as the CFD models to validate your simulation theory?
In Figure 5, you clearly showed the boundary of humping and no humping by simulation. However, it is better if you can re-do the experiments to validate these simulation estimations.
Previous studies have investigated the humping phenomenon using high-speed optical cameras [6–8] or X-ray imaging equipment with a lower frame rate (e.g., 1000 fps in [4]) compared to the 20,000 fps synchrotron X-ray imaging we used. For laser welding, 20,000 fps is still low due to the speed of the laser spot, but for plasma welding, 1000 fps is sufficient for calculations with proper calibration and literature-based discussion. The number of frames used depends on the specific process.

In some figures, the scale bar and number are not clear or not mentioned.

Reviewer #2

(Remarks to the Author)
Overall, the authors have answered most questions I raised. Please also comment about the dissimilar bonding by using this possible future modification in modeling and it is not mandatory. Yes, it is worthy to be published in this Journal.

Version 2:

Reviewer comments:

Reviewer #1

(Remarks to the Author)
Thank you for your effort in revising the manuscript. You've addressed most of my questions, and I'm satisfied with your responses. However, I have a few comments where it seems there may have been some misunderstandings.
For instance, in Table 3, you compare experimental and simulation results, but it's unclear how and where you obtained the experimental data. Did you conduct the experiments yourself, or were the results cited from other papers?
If the data was cited from other papers, please verify that the source/paper used two X-ray sources, as the use of only one X-ray source would result in 2D images and videos, which could lead to incorrect velocity measurements. If the data was from other groups, please ensure you are citing studies that used two X-ray sources.
If the experiment was conducted by your team, how was the velocity measured? A velocity of 6 m/s seems unusually high, and it might be unrealistic. It would be beneficial to discuss this value in the context of previously published papers. For example, I have read papers by Prof. Katayama on laser welding, and his measured velocities don't seem to reach 6 m/s. Please make sure this is addressed properly.
As for Comment C5, please refer to the paper I provided. I apologize if there were any difficulties in accessing it.
Title paper: Undercut Formation Mechanism in Keyhole Plasma Arc Welding
Link: https://s3.amazonaws.com/WJ-www.aws.org/supplement/2019.98.018.pdf

Version 3:

Reviewer comments:

Reviewer #1

(Remarks to the Author)
Thank you for your reply.
I'm okay with most of your response. However, I find the additional sentences you included in the manuscript unclear. I believe it's widely understood that using a single X-ray source from a side view can only produce 2D projected images and videos, making it impossible to calculate velocity within the melt pool.
I agree that you should clearly state that using one X-ray source, as referenced in the published papers, makes velocity calculation impossible. As you mentioned, the term "projected velocity" doesn't apply here. It is impossible to calculate velocity without sufficient data from the X, Y, and Z axes. Therefore, I suggest you explicitly mention in your paper that calculating the flow velocity in the melt pool with just one X-ray source is not feasible. Additionally, the melt pool is extremely small, making it highly challenging to use W or Ta particles, which is why you opted to use the CFD model.
In fact, the issue with a small melt pool is just one aspect of the challenge. The core issue, as in references 34–36 and in your paper, is that it's impossible to calculate velocity with a single X-ray source, so using a CFD model to make predictions is a reasonable approach.
Please consider this and your paper can be published.

Response Letter

Thank you for your letter concerning our manuscript (NCOMMS-24-15270) entitled "Unveiling Mechanisms and Onset Threshold of Humping in High-Speed Laser Welding". Those comments are valuable and helpful for improving our paper. We have read the comments carefully and revised the manuscript accordingly. Please see below the Authors' point-to-point answers (A) to the Reviewers' comments (C).

Note: The colors of the text correspond to responses to Reviewer #1 – Color 1 and Reviewer #2 – Color 2. Other revisions – Color 3.

Reviewer #1

Thank you for your insightful suggestions. We have thoroughly considered and addressed your comments in this revised manuscript. The response to each comment is detailed below:

C1: In the introduction, it would be beneficial to highlight potential applications for the investigation of ultra-thin sheets. For instance, ultra-thin sheets find relevance in various industries such as the manufacturing of lead frames for semiconductors, radiators for automotive applications, lithium batteries for electric vehicles, as well as in motors and stators. These applications signify the importance of understanding the behavior of ultra-thin sheets, as highlighted in research studies such as those mentioned in the link provided.

While I don't require you to cite this paper, it's evident that this paper represents one of the few instances discussing applications of extremely thin sheets for welding.

https://www.sciencedirect.com/science/article/pii/S1526612522004261

If due to the limitations of X-ray photon sources, I recommend considering conducting this type of experiment at the ESRF in France. They possess significantly higher power capabilities, enabling experimentation with thicker plates.

A1: Thank you for your valuable suggestion. The welding of metal foils is crucial in several applications, such as motor rotors [1], electronic device connectors [1], and automobile fuel cells [2]. In this study, the focus is on fuel cell fabrication. Using thin materials for bipolar plates reduces weight and cost [2], decreases thermal mass and stack size [2], and enables more complex designs

[3], thereby improving fuel cell performance. The introductions have been updated in the manuscript, with the mentioned references included (Pages 1–2, Lines 28–33):

"The laser welding process offers several advantages, including a small heat-affected zone, fast welding speed, and high flexibility in welding path design [1]. These benefits make it well-suited for fuel cell fabrication, which requires long and narrow welding paths between bipolar plates [2,3]. Thin foils are preferred for these plates as they can reduce weight [4] and enable more complex channel designs [5]. Welding metal foils is also applied in other applications such as motor rotors and electronic device connectors [6]."

Additionally, thank you for introducing the capabilities of ESRF in France. We will keep in mind to use the facility by taking advantage of the higher-power X-rays.

C2: On the other hand, let's delve into the humping phenomenon using X-ray or high-speed camera techniques for welding. Despite the abundance of literature on welding, joining, and additive manufacturing with similar mechanisms, exemplified by papers from Dr. Nguyen Van Anh (https://www.sciencedirect.com/science/article/pii/S1526612520306885) or Prof. ChuanSong Wu on plasma arc welding, the phenomena discussed in your paper are not groundbreaking. The mechanisms you address are well-known. However, the novelty in your research lies in its application to very ultra-thin sheets. Additionally, you've conducted supplementary simulations to provide evidence and validation, distinguishing your work from existing studies.

A2: Thank you for your comment. We have included the references mentioned [4,5], which corresponds to ref. [25,26] in the revised manuscript (Page 3, Line 56). Humping is a known defect in high-speed laser welding and laser-based additive manufacturing. Previous studies have investigated the humping phenomenon using high-speed optical cameras [6–8] or an X-ray imaging equipment with a lower frame rate (e.g., 1000 fps in [4]) compared to the synchrotron X-ray imaging (20,000 fps) we used. However, these methods are insufficient to directly observe keyhole dynamics. Computational fluid dynamics (CFD) simulations also lack direct experimental validation for the size of the molten pool.

Our manuscript identifies humping mechanisms using in situ high-speed synchrotron X-ray imaging for direct keyhole observation (experimental ground truth data) and CFD simulations to understand fluid characteristics. We also introduce a dimensionless humping index to predict the onset of humping, validated by our data and existing literature. This work provides a deep understanding of humping mechanisms, distinguishing it from previous studies.

C3: Regarding the velocity claim of exceeding 6 m/s, it's crucial to provide more evidence or validation for this value. Is there sufficient data to support its accuracy?

Including a scale in Figures 2 and 3 would greatly enhance clarity and aid in interpretation.

A3: Thank you for the valuable comment. We recorded X-ray images during laser welding along with the corresponding instantaneous time, allowing us to calculate the actual welding speed from the in-situ X-ray videos (Supplementary Movies 1–5). The welding speeds calculated from the videos are consistent with the set speeds. The manuscript has been revised accordingly (Page 5, Lines 108–110):

"For a comprehensive view of all in situ observations for five different welding speeds, refer to Supplementary Movies 1-5. The moving speed of keyhole recorded during the in situ observations was consistent with the set welding speed."

Additionally, the scales in Figures 2 and 3 (Pages 8 and 9) have been revised for better clarity, with corresponding values provided in the figure captions as per the journal's format.

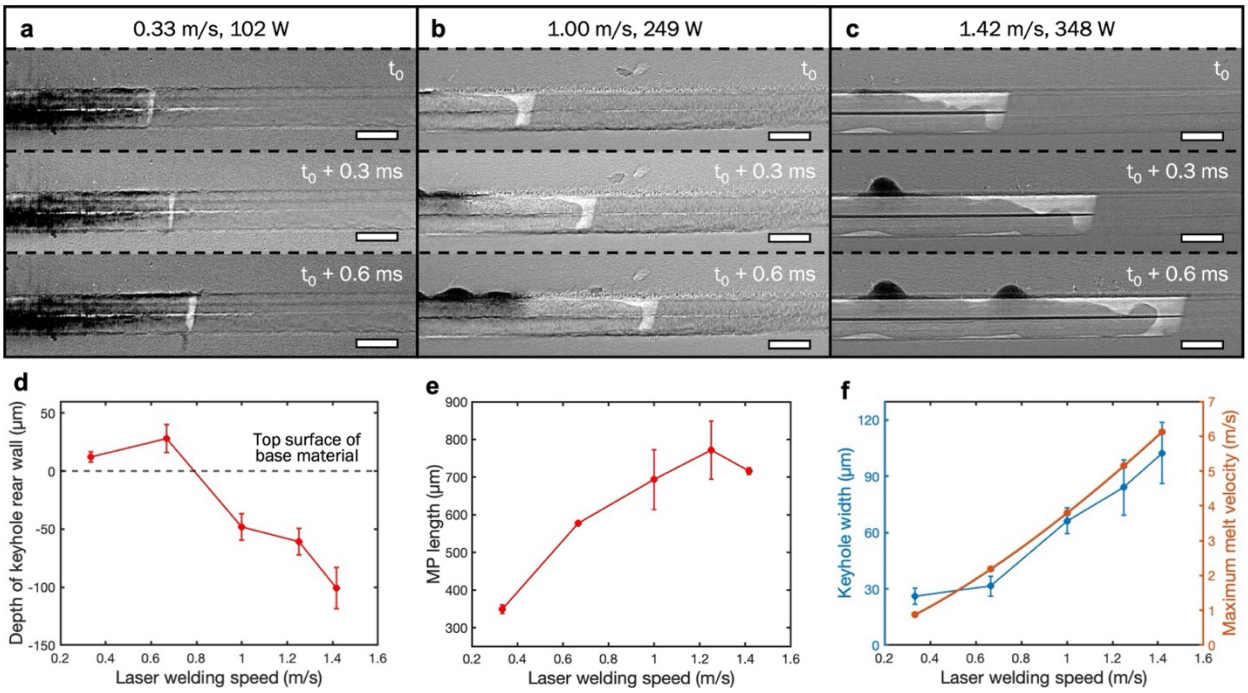

Fig. 2 **a–c** In situ high-speed synchrotron X-ray observations of laser welding at the welding speeds of 0.33, 1.00, and 1.42 m/s at the arbitrary times of t_0, $t_0 + 0.3$, and $t_0 + 0.6$ ms. All scale bars are 200 μm. See Supplementary Movies 1–5 for in situ observations at five different welding speeds. **d** Depth of keyhole rear wall. **e** MP length. **f** Keyhole width (measured) and maximum melt velocity (calculated by Equation 1).

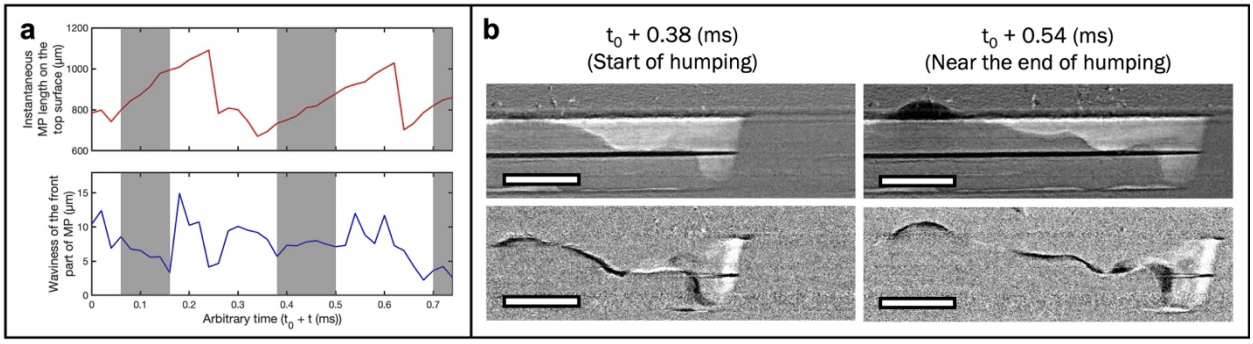

Fig. 3 Analysis of humping cycle at the welding speed of 1.42 m/s. **a** MP length on the top surface and waviness of the front part of MP, with the starting periods of humping marked in grey. **b** Examples of MP waviness changes during humping. At the start of humping ($t_0 + 0.38$ ms), the average MP waviness was lower. Near an end ($t_0 + 0.54$ ms), the MP surface showed higher waviness because of the steeper gradient of the backward melt flow's volumetric rate. All scale bars = 200 μm.

C4: Could you please elaborate on the welding process used for joining the two plates? Specifically, did you utilize a butt-joint or an overlap joint? If an overlap joint was employed, please provide detailed information. Additionally, it would be beneficial to provide more comprehensive details about the X-ray system, parameters, and experimental setup. Including images of the experimental setup could significantly improve understanding, particularly considering the challenges associated with working with very ultra-thin sheets and utilizing X-ray technology.

A4: Thank you for pointing this out. The laser welding setup involved overlapping two vertically stacked metal foils and welding them from the top. An in-house Al alloy fixture, chosen for its lower X-ray attenuation compared to steel [9], was designed to clamp the foils and prevent movement, with a 300 μm-wide opening for the laser. Supplementary Fig. 1b includes a picture to illustrate the experimental setup. The manuscript has been revised accordingly (Pages 17–18, Lines 334–343):

"In situ high-speed synchrotron X-ray imaging of laser welding was conducted at beamline 32-ID-B at ANL using an ytterbium single-mode continuous wave laser source (YLR-500-AC). The experimental setup is presented in Supplementary Fig. 1a–b. The laser welding configuration involved overlapping two vertically stacked stainless steel foils welded from the top. An Al alloy fixture was designed to clamp the foils and prevent movement, featuring a 300 μm-wide opening for the laser (Supplementary Fig. 1b). The Al alloy was chosen for its lower X-ray attenuation compared to steel [47]. A pseudo pink X-ray beam, with the 1st harmonic energy at 24.7 keV, was

generated using an 18 mm undulator and directed through the sample from the side during the laser welding process. ”

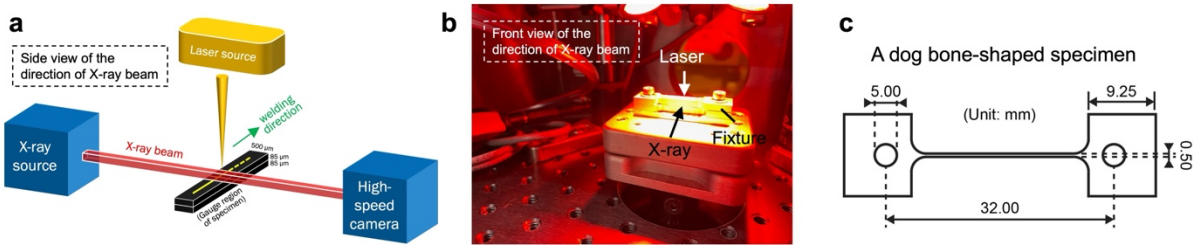

Supplementary Fig. 1 Experimental setup of in situ high-speed synchrotron X-ray imaging at ANL. **a** The side and **b** the front views of the direction of X-ray beam. The laser welding configuration was an overlapped weld. **c** Geometry of the dog bone-shaped specimen. Narrow width (500 μm) in the gauge region is required due to the strong attenuation of X-ray on stainless steel.

C5: Given the difficulty of setting up experiments with ultra-thin sheets and the similarities with X-ray technology, discussing any novel insights or differences compared to results obtained with thicker materials would be valuable. Discuss these differences by cite other papers could make a substantial contribution to the fields of welding, joining, and additive manufacturing, particularly at the microscale thickness level, where most researchers focus on thicker materials.

A5: Thank you for this valuable comment. One difference between welding thin and thick samples is the required power density. Since we have entered the "keyhole" regime in this experiment, the keyhole dynamics would not vary significantly, which was also confirmed by other literatures [10,11]. Another difference is the absence of keyhole-induced porosity because of the use of thin foils in this study. This type of pore forms when bubbles are unable to escape before solidification in a deep keyhole [10,12,13]. The manuscript has been updated accordingly (Page 5, Lines 114–115):

“It is worth noting that the use of thin foils in this study prevented the formation of deep keyholes and deep-keyhole-induced porosity observed in other literatures [29,30,33].”

Reviewer #2

Thanks for your valuable suggestions. Your comments have been thoroughly considered and addressed in this revised manuscript. The response to each comment is listed below:

C1: The data shown in Fig.1 (b) and (c) are so coherent. Reviewers also would like to see the comparisons between the simulation and experimental data in the average height of humpings.

A1: Thank you for your comment. We have included the simulated hump height data in the revised manuscript. The simulated average height of the humps (53.75 ± 11.11 μm) closely matched the experimental observations (58.70 ± 14.82 μm), with a difference of 8.4%. The manuscript has been updated accordingly (Page 20, Lines 396–398):

"The average height of the humps closely matched between the simulation (53.75 ± 11.11 μm) and experimental observations (58.70 ± 14.82 μm) with an 8.4% difference."

It is also noted that the height of the humps was measured relative to the weld top surface, and the caption of Fig. 1c has been updated.

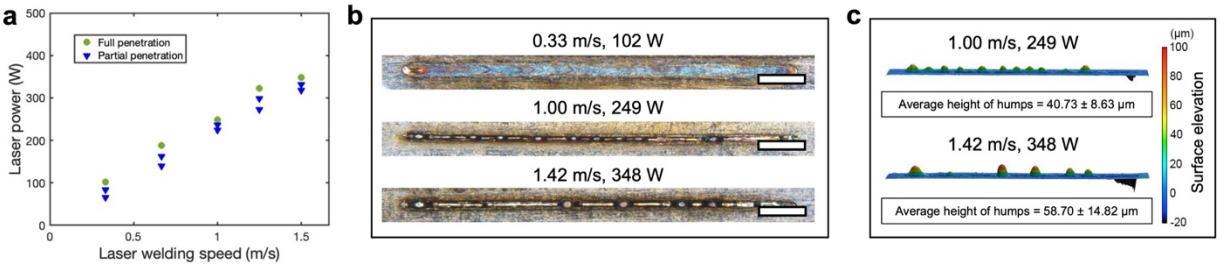

Fig. 1 **a** The corresponding laser power at each welding speed was determined at EWI by incrementally increasing the laser power until full penetration was achieved. **b** Top surfaces of weld seams at the welding speeds of 0.33, 1.00, and 1.42 m/s. Note that the fastest speed was adopted as 1.42 m/s instead of 1.50 m/s due to the equipment setup at ANL. All scale bars correspond to 500 μm. **c** Surface topography of weld seams at 1.00 and 1.42 m/s, and the average hump height relative to the weld top surface.

C2: In your modeling, was the surface or volumetric heat source used? It matters to your simulation results and please explain why you chose one of them.

A2: Thank you for your valuable comment. In the CFD simulation model, a surface heat source was employed because it is an effective approach to simulate laser-material interaction at the material's surface. This method is also commonly used in other studies [14–19]. In this setup, the heat flux was divided into rays for each mesh according to a Gaussian distribution. Each ray was reflected and absorbed based on the absorption rate when it hit the metal surface [17]. This information has been included in the revised manuscript (Page 19, Lines 378–382):

"The laser beam, with a spot diameter of 43 μm, was considered a surface heat source, a method commonly used in other studies [9,18,38,48–50] to simulate laser-material interaction. In this heat source, the heat flux was divided into each mesh, following the Gaussian distribution shown in Supplementary Fig. 3b. The laser beam was reflected and absorbed based on the material absorptivity [48]."

C3: MW, what unknown parameters that you use for experimental fitting? Or you did not use the fitting way between simulation and experimental data? All need to be explained in detail.

A3: Thank you for pointing this out. The experimental fitting ($l \propto P/u_w^{\frac{1}{2}} r^{\frac{3}{4}}$ in Equation 4) was determined by identifying the combinations of exponents for power (P), laser welding speed (u_w), and spot radius (r) that yielded the highest R^2 value. The data were obtained from our current study and other literatures [20,21]. We did not extract the data from simulation for fitting, because we believe the experimental data is the ground truth.

The manuscript has been revised accordingly to enhance the clarity (Page 14, Lines 270–275):

"The scaling of MP length has not been previously reported due to its requirement of in situ observation. In this work, linear fitting was performed with experimental data and literature data [8,44], as shown in Fig. 5a, following the equation:

$$l \propto P/u_w^{\frac{1}{2}} r^{\frac{3}{4}} \quad (4)$$

This relationship has the highest R^2 value (0.9856) among all exponent combinations for each process parameter."

C4: Please list a table to illustrate all the numbers that you set in those unknown parameters. Are those temperatures independent or dependent? For example, thermal conductivity, surface tension coefficient, recoil pressure.....

A4: Thank you for pointing out this issue in the original manuscript. Supplementary Fig. 4 and Supplementary Table 1 have been added to present the numbers used in this study.

In the CFD simulation, the thermophysical properties (density, specific heat, thermal conductivity, viscosity, and surface tension) were temperature-dependent, which were obtained from the databases [16,22] (Supplementary Fig. 4). The recoil pressure was also temperature-dependent, following $P_{recoil} = a \exp\left[b\left(1 - \frac{T_b}{T}\right)\right]$ with a = 11000 Pa and b = 6 [23]. For simplicity, the materials constants in the dimensionless humping index (Equations 1–3 and 5) were considered temperature-independent (Supplementary Table 1).

The manuscript has been revised accordingly (Pages 14–15, Lines 279–281):

"The values of ρ, c_p, k, and γ were obtained at T_m from the thermophysical databases [38,39], as listed in Supplementary Table 1. Both u_{max} and l were obtained from Equations 1 and 4, respectively, rather than from the simulation results."

(Page 20, Lines 387–388):

"The temperature-dependent laser absorptivity data were acquired from reference [51], and the temperature-dependent physical properties were obtained from references [38,39], as shown in Supplementary Fig. 4. The recoil pressure was temperature-dependent, following $P_{recoil} = a \exp\left[b\left(1 - \frac{T_b}{T}\right)\right]$ with a = 11000 Pa and b = 6 [52]."

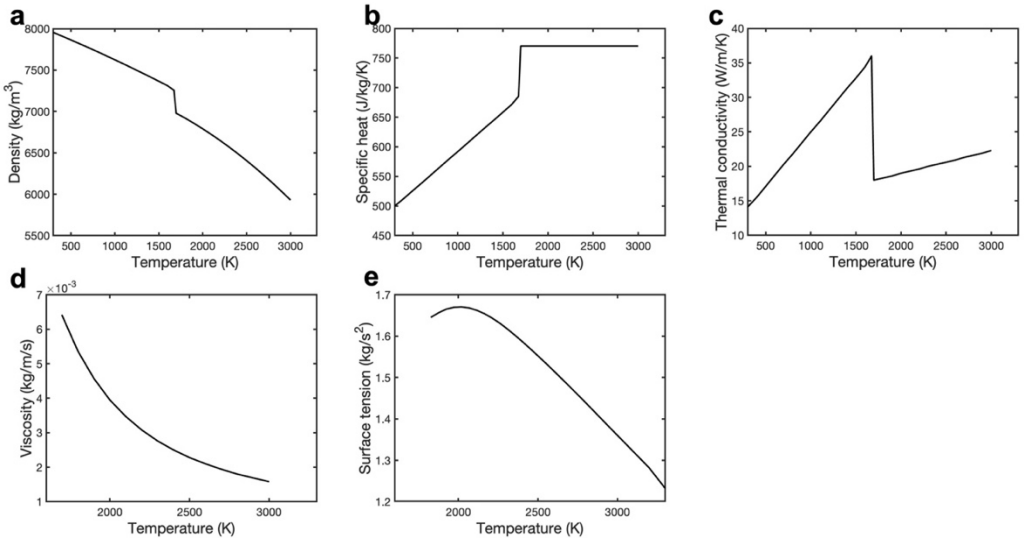

Supplementary Fig. 4 Thermophysical properties used in the CFD simulation, including **a** density, **b** specific heat, **c** thermal conductivity, **d** viscosity, and **e** surface tension. They were obtained from references [38,39].

Supplementary Table 1 Materials constants used in Equation 1–3 and 5. These constants were extracted from the thermophysical properties, as shown in Supplementary Fig. 4.

Material's Properties	Values at T_b	Values at T_m
Density (ρ)	$6000\ \frac{kg}{m^3}$	$7000\ \frac{kg}{m^3}$
Thermal conductivity (k)	$25\ \frac{W}{m \cdot K}$	$25\ \frac{W}{m \cdot K}$
Specific heat (c_p)	$796.2\ \frac{J}{kg \cdot K}$	$796.2\ \frac{J}{kg \cdot K}$
Boiling temperature (T_b)	$3134\ K$	
Melting temperature (T_m)	$1698\ K$	
Ambient temperature (T_0)	$300\ K$	
Latent heat of fusion (L_m)	$2.6 \times 10^5\ \frac{J}{kg}$	

C5: Several papers have mentioned about the humping due to Rayleigh's instability. From the simulation results, you even add more explanations in humping, for example, the shorter keyhole rear wall, ..., however in your simulation, could you see the humping cycle? To me, the humping will happen all the time in your modeling, am I right? Just as you mentioned, the humping cycle was analyzed with several "instantaneous" MP characteristics. The observation aligned well with the humping theory based on the conservation of volume. Please explain it in detail.

A5: Thank you for your valuable suggestion. You are correct. Humping does not occur continuously but rather forms periodically. To illustrate this characteristic, we examined the differences in net cross-sectional volumetric flow rates between the start and end of humping in a humping cycle from the simulation at 1.42 m/s (Fig. 4c). It can be concluded that Humping occurs periodically rather than continuously due to alternating excessive melt accumulation at the start and molten pool length extension near the end. We have revised the manuscript and Fig. 4c accordingly (Page 11, Lines 213–225):

"At the welding speed of 1.42 m/s, flow rates were analyzed at the start and near the end of humping to understand its periodic nature. At the start (blue curve in Fig. 4c), the entire MP length (1050 μm) showed a significant net backward volumetric flow in the front 1000 μm, causing severe melt accumulation at the MP tail. The gradient of the volumetric flow rate decreases from the front to the end, indicating the elongated MP tail cannot effectively decelerate the backward melt flow, which is attributed to the shallow inclination angle of the MP boundary tail (Fig. 4b). A long MP tail also suggests a strong humping tendency due to the Rayleigh instability [20,21]. Conversely, near the end of humping (orange curve in Fig. 4c), the MP length was about 250 μm longer than that at the start, providing more volume in the MP tail to accommodate the melt. The MP tail had a net volumetric flow rate close to zero (enlarged view in Fig. 4c), indicating insignificant melt accumulation, causing a gradual stop of humping. This periodic humping, characterized by alternating melt accumulation and MP length extension, aligns with the conservation of volume [8]."

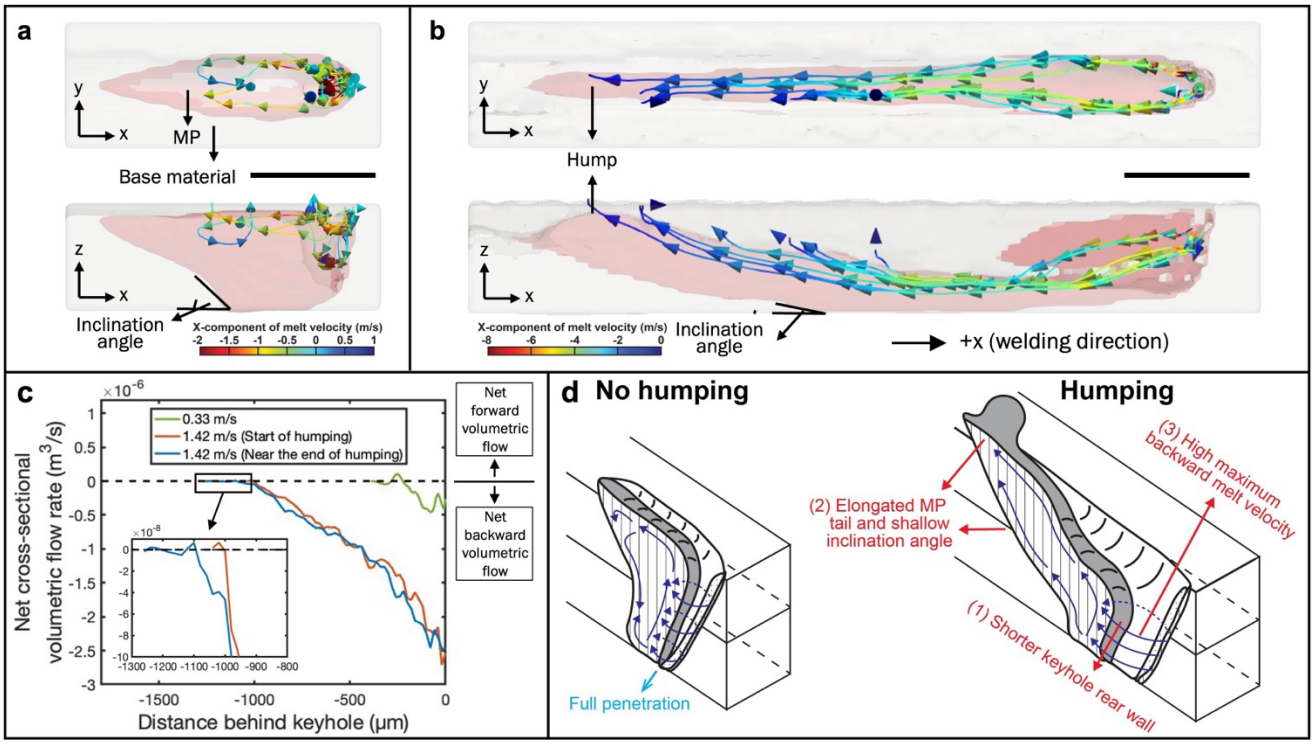

Fig. 4 **a–b** Top and side views of streamlines extracted from CFD simulation results at welding speeds of 0.33 and 1.42 m/s. All scale bars correspond to 200 μm. **c** Net cross-sectional volumetric flow rate extracted from different distances of y-z cross-sections behind the keyhole at the welding speeds of 0.33 m/s, 1.42 m/s (start of humping), and 1.42 m/s (near the end of humping). An enlarged view highlights the curves around the MP tail at 1.42 m/s. **d** Schematic diagram showing the formation mechanisms of humping.

C6: I just wonder if the no-humping zone is optimal in mechanical properties in bonding. Please confirm if the mechanical properties such as shear strength, porosity,..... in bonding are better. To me, the no-humping zone is only for those parameters without humping, but the qualities of the bonding still need to study furthermore.

A6: Thank you for your comment. Weld strength is crucial in fuel cell applications to ensure that the bipolar plates are welded strongly enough to hold the liquid or gas between them. In this research, we evaluated the mechanical properties of these laser welds using T-peel tests to present the common loading condition of the bipolar plates, and the results are included in Supplementary Fig. 2. The strength can reach approximately 30 N/mm for the welds made at 0.67 m/s when

humping does not occur. It decreases as the welding speed increases further because of the formation of humps.

These results have been incorporated into the revised manuscript (Page 4, Lines 93–97):

"On the other hand, the T-peel strengths of the welds (defined as the load per unit length of weld) were tested following the configuration in refs. [31,32]. Laser welds made at EWI were used because the sample size for in-situ X-ray imaging was too small for mechanical testing. The results, presented in Supplementary Fig. 2, indicate that the T-peel strength decreased when the welding speed exceeded 1.00 m/s due to the formation of humping."

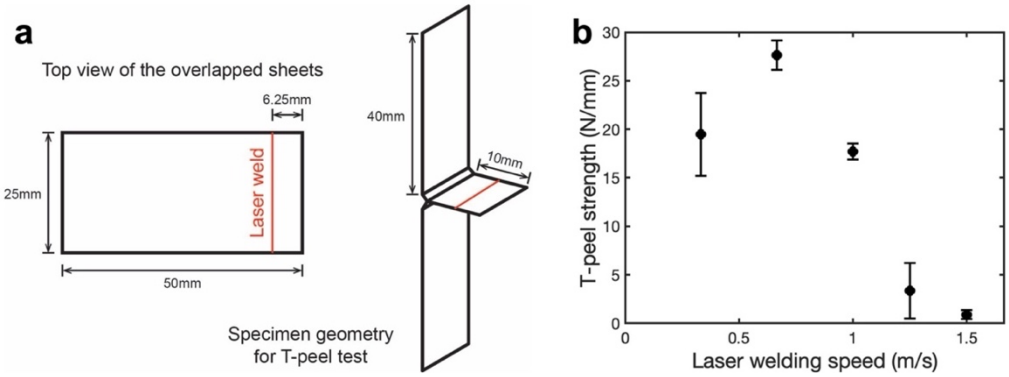

Supplementary Fig. 2 **a** The configuration of laser welds made in EWI and the specimen geometry for T-peel test, which followed refs. [31,32]. **b** T-peel strengths of laser welds (defined as the load per unit length of weld). The T-peel strength gradually decreased when the welding speed exceeded 1.00 m/s due to the formation of humping.

C7: Finally, is it possible to use the hybrid manufacturing way to cool down the tail of melting pool at once to suppress humping? Please comment.

A7: Yes, we believe it is possible to suppress humping through hybrid manufacturing methods. Although we have not yet studied these hybrid methods, the dimensionless humping index (π_h) developed in this study suggests potential approaches to mitigate humping in a single laser system. The key strategy is to reduce π_h, which can be achieved by reducing spot radius, decreasing base material thickness, and utilizing an adjustable ring mode laser [24,25].

Further discussions on the effective of each approach on π_h can be found in the revised manuscript (Pages 15–16, Lines 291–305):

"The intersection points between each penetration depth and the 10,000-isoline of π_h represent the critical laser welding speeds and power. The model suggests several methods to enhance the critical laser welding speed for the same material system by reducing π_h. The first approach is to employ a finer r, which requires a lower P for the same penetration depth. As a result, both u_{max} and l decrease, as indicated by Equations 1 and 4, leading to a reduced π_h and an increased critical laser welding speed. By comparing the contour maps between Fig. 5c and Fig. 5d, it is evident that the critical welding speed increases from 0.53 to 0.66 m/s when r is reduced from 50 to 25 μm. The second approach is to reduce the thickness of the base material, which lowers the required P for full penetration and consequently decreases π_h because of the reduced u_{max} and l (Equations 1 and 4). As shown in Fig. 5c, the critical welding speed increases from 0.44 to 0.53 m/s at r=50 μm when the thickness is reduced from 300 to 150 μm. The third approach is to employ an adjustable ring mode laser [45,46], where a portion of the power is distributed to the outer ring. It allows the power of the central beam to be decreased while maintaining the same penetration depth, leading to a shorter l (Equation 4), a reduced π_h, and therefore a greater critical laser welding speed."

References

[1] N.H. Manh, V.A. Nguyen, H. Le Duy, M. Akihisa, V.T. Le, T.Q. Ngoc, B. Gandham, Development of a novel GTAW process for joining ultra-thin metal sheets, J Manuf Process 80 (2022) 683–691. https://doi.org/https://doi.org/10.1016/j.jmapro.2022.06.043.

[2] H. Tawfik, Y. Hung, D. Mahajan, Metal bipolar plates for PEM fuel cell—A review, J Power Sources 163 (2007) 755–767. https://doi.org/https://doi.org/10.1016/j.jpowsour.2006.09.088.

[3] M.M. Barzegari, F.A. Khatir, Study of thickness distribution and dimensional accuracy of stamped metallic bipolar plates, Int J Hydrogen Energy 44 (2019) 31360–31371. https://doi.org/https://doi.org/10.1016/j.ijhydene.2019.09.225.

[4] A. Van Nguyen, S. Tashiro, M.H. Ngo, H. Van Bui, M. Tanaka, Effect of the eddies formed inside a weld pool on welding defects during plasma keyhole arc welding, J Manuf Process 59 (2020) 649–657. https://doi.org/https://doi.org/10.1016/j.jmapro.2020.10.020.

[5] L. Wang, C. Wu, J. Chen, J. Gao, Influence of the external magnetic field on fluid flow, temperature profile and humping bead in high speed gas metal arc welding, Int J Heat Mass Transf 116 (2018) 1282–1291. https://doi.org/https://doi.org/10.1016/j.ijheatmasstransfer.2017.09.130.

[6] Y. Ai, P. Jiang, C. Wang, G. Mi, S. Geng, W. Liu, C. Han, Investigation of the humping formation in the high power and high speed laser welding, Opt Lasers Eng 107 (2018) 102–111. https://doi.org/https://doi.org/10.1016/j.optlaseng.2018.03.010.

[7] R. Fabbro, Melt pool and keyhole behaviour analysis for deep penetration laser welding, J Phys D Appl Phys 43 (2010) 445501. https://doi.org/10.1088/0022-3727/43/44/445501.

[8] B. Xue, B. Chang, D. Du, Monitoring of high-speed laser welding process based on vapor plume, Opt Laser Technol 147 (2022) 107649. https://doi.org/https://doi.org/10.1016/j.optlastec.2021.107649.

[9] D.F. Jackson, D.J. Hawkes, X-ray attenuation coefficients of elements and mixtures, Phys Rep 70 (1981) 169–233. https://doi.org/https://doi.org/10.1016/0370-1573(81)90014-4.

[10] Y. Huang, T.G. Fleming, S.J. Clark, S. Marussi, K. Fezzaa, J. Thiyagalingam, C.L.A. Leung, P.D. Lee, Keyhole fluctuation and pore formation mechanisms during laser

powder bed fusion additive manufacturing, Nat Commun 13 (2022) 1170. https://doi.org/10.1038/s41467-022-28694-x.

[11] R. Cunningham, C. Zhao, N. Parab, C. Kantzos, J. Pauza, K. Fezzaa, T. Sun, A.D. Rollett, Keyhole threshold and morphology in laser melting revealed by ultrahigh-speed x-ray imaging, Science (1979) 363 (2019) 849–852. https://doi.org/10.1126/science.aav4687.

[12] C. Zhao, N.D. Parab, X. Li, K. Fezzaa, W. Tan, A.D. Rollett, T. Sun, Critical instability at moving keyhole tip generates porosity in laser melting, Science (1979) 370 (2020) 1080–1086. https://doi.org/10.1126/science.abd1587.

[13] M. Bayat, A. Thanki, S. Mohanty, A. Witvrouw, S. Yang, J. Thorborg, N.S. Tiedje, J.H. Hattel, Keyhole-induced porosities in Laser-based Powder Bed Fusion (L-PBF) of Ti6Al4V: High-fidelity modelling and experimental validation, Addit Manuf 30 (2019) 100835. https://doi.org/https://doi.org/10.1016/j.addma.2019.100835.

[14] B. Xue, B. Chang, S. Wang, R. Hou, P. Wen, D. Du, Humping Formation and Suppression in High-Speed Laser Welding, Materials 15 (2022). https://doi.org/10.3390/ma15072420.

[15] C. Tang, K.Q. Le, C.H. Wong, Physics of humping formation in laser powder bed fusion, Int J Heat Mass Transf 149 (2020) 119172. https://doi.org/https://doi.org/10.1016/j.ijheatmasstransfer.2019.119172.

[16] N. Chen, H.A. Khan, Z. Wan, J. Lippert, H. Sun, S.-L. Shang, Z.-K. Liu, J. Li, Microstructural characteristics and crack formation in additively manufactured bimetal material of 316L stainless steel and Inconel 625, Addit Manuf 32 (2020) 101037. https://doi.org/10.1016/j.addma.2020.101037.

[17] M. Dal, R. Fabbro, [INVITED] An overview of the state of art in laser welding simulation, Opt Laser Technol 78 (2016) 2–14. https://doi.org/https://doi.org/10.1016/j.optlastec.2015.09.015.

[18] W.-I. Cho, S.-J. Na, C. Thomy, F. Vollertsen, Numerical simulation of molten pool dynamics in high power disk laser welding, J Mater Process Technol 212 (2012) 262–275. https://doi.org/https://doi.org/10.1016/j.jmatprotec.2011.09.011.

[19] Y. Lee, D.F. Farson, Simulation of transport phenomena and melt pool shape for multiple layer additive manufacturing, J Laser Appl 28 (2015) 012006. https://doi.org/10.2351/1.4935711.

[20] P. Berger, H. Hügel, A. Hess, R. Weber, T. Graf, Understanding of Humping Based on Conservation of Volume Flow, Phys Procedia 12 (2011) 232–240. https://doi.org/10.1016/j.phpro.2011.03.030.

[21] T. Lei, Y. Rong, J. Xu, Y. Huang, Experiment study and regression analysis of molten pool in laser welding, Opt Laser Technol 108 (2018) 534–541. https://doi.org/https://doi.org/10.1016/j.optlastec.2018.07.053.

[22] C.S. Kim, Thermophysical properties of stainless steels, United States, 1975. https://doi.org/10.2172/4152287.

[23] Z. Wan, H.-P. Wang, J. Li, J. Solomon, Y. Zhu, B. Carlson, Novel measures for spatter prediction in laser welding of thin-gage zinc-coated steel, Int J Heat Mass Transf 167 (2021) 120830. https://doi.org/https://doi.org/10.1016/j.ijheatmasstransfer.2020.120830.

[24] L. Wang, X. Gao, F. Kong, Keyhole dynamic status and spatter behavior during welding of stainless steel with adjustable-ring mode laser beam, J Manuf Process 74 (2022) 201–219. https://doi.org/https://doi.org/10.1016/j.jmapro.2021.12.011.

[25] J. Li, P. Jiang, S. Geng, J. Xiong, Numerical and experimental study on keyhole dynamics and pore formation mechanisms during adjustable-ring-mode laser welding of medium-thick aluminum alloy, Int J Heat Mass Transf 214 (2023) 124443. https://doi.org/https://doi.org/10.1016/j.ijheatmasstransfer.2023.124443.

Response Letter

Thank you for your letter concerning our revised manuscript (NCOMMS-24-15270A) entitled "Unveiling Mechanisms and Onset Threshold of Humping in High-Speed Laser Welding". Those comments are valuable and helpful for improving our paper. We have read the comments carefully and revised the manuscript accordingly. Please see below the Authors' point-to-point answers (A) to the Reviewers' comments (C).

Note: The colors of the text correspond to responses to Reviewer #1 – Color 1 and Reviewer #2 – Color 2.

Reviewer #1

Thank you for your insightful suggestions, which have been instrumental in improving our manuscript. We have carefully addressed each of your comments in this revised version. Detailed responses to each comment are provided below.

C1: The humping phenomenon is significantly related to the velocity of fluid flow in the melt pool, the behavior of convection patterns, and the appearance of eddies. Discuss more details in quantity based on velocity change is must better.

A1: Thank you for valuable comment. The authors agree that the velocity of fluid flow, the behavior of the convection patterns, and the appearance of eddies are crucial. To analyze them, we extracted the velocity of fluid flow in molten pool (MP) (Fig. 4a–b) from the CFD simulations. The convection pattern was visualized by the streamline at the same time (Fig. 4a–b). We further quantitatively analyzed the net cross-sectional volumetric flow rate (Fig. 4c). In our work, they were not directly analyzed by adding W tracer particles in the synchrotron X-ray imaging because of the following technical challenges. First, due to the thin and narrow sheets used in this study (Supplementary Fig. 1c), properly placing the W particles between the sheets was challenging. Second, the fine laser spot size (43 μm) resulted in a MP width of approximately 80–100 μm. Given that the available W particle size is roughly 10–20 μm, the particles either could not enter the MP or would significantly affect the keyhole dynamics and the laser welding process. Actually, we did try to add W particles to track the material flow, but it wasn't successful for the above reasons. The formation of eddies was also unachievable due to the necessity of tracer particles. We noticed that other researchers achieved success in the arc welding process [1,2] because of the larger spot size (wider molten pool) compared to this study, and in laser powder bed fusion [3,4], where the tracer particles can be premixed with the powder bed.

From the CFD simulation results, we extracted streamlines to comprehend the velocity of fluid flow in the melt pool and the behavior of convection patterns. When humping did not occur at the welding speed of 0.33 m/s (Fig. 4a), the melt could return to the MP before the solidification front reached it. However, when humping occurred (Fig. 4b) at the welding speed of 1.42 m/s, the melt flow traversed the entire MP, accumulated at the MP tail, and formed a hump, as indicated by the blue streamlines.

We further analyzed the net cross-sectional volumetric flow rates (Fig. 4c), defined as the flow rates across the y-z cross sections (+x is the welding direction). It considers the effects of both melt velocity and melt volume and provides a quantitative assessment of melt accumulation toward the MP tail. A negative value indicates that the net volumetric flow rates is in the -x direction (opposite to the laser welding direction). It was found that when humping occurred at 1.42 m/s (orange and blue curves in Fig. 4c), the front of MP exhibited a significantly more negative volumetric flow rate ($\sim -2.4 \times 10^{-4} m^3 s^{-1}$) compared to that when humping did not form at 0.33 m/s ($\sim -5.5 \times 10^{-5} m^3 s^{-1}$, green curve in Fig. 4c). In addition, the negative volumetric flow rate extended all the way to the MP tail. These results indicate significant melt accumulation, leading to humping.

We added more discussions on the velocity change in MP in the revision (Page 10, Lines 201–206):

"At the welding speed of 0.33 m/s (Fig. 4a), the melt flow gradually diminished to zero at roughly the midpoint of MP and then re-entered the MP before the solidification front reached it. In contrast, at the welding speed of 1.42 m/s (Fig. 4b), the melt flow remained directed backward and could not return to the MP, so it eventually traversed the entire MP length and be deflected upward to form hump (as highlighted in the blue streamlines)."

The manuscript has also been revised for the quantitative analyses of volumetric flow rates (Page 11, Lines 207–214):

"The net cross-sectional volumetric flow rate (Fig. 4c), defined as the flow rates across the y-z cross sections (+x is the welding direction), accounts for the effects of melt velocity and melt volume. It provides quantitative assessment backward melt accumulation toward the MP tail. A negative value indicates that the net volumetric flow rates is in the -x direction (backward). At the welding speed of 0.33 m/s, the flow rate was relatively low ($\sim -5.5 \times 10^{-5} m^3 s^{-1}$) at the front of the MP and nearly zero at the MP tail. At the welding speed of 1.42 m/s, the flow rate became more negative ($\sim -2.4 \times 10^{-4} m^3 s^{-1}$) at the front of the MP and remained negative across the entire MP, indicating greater melt accumulation toward the MP tail and leading to humping."

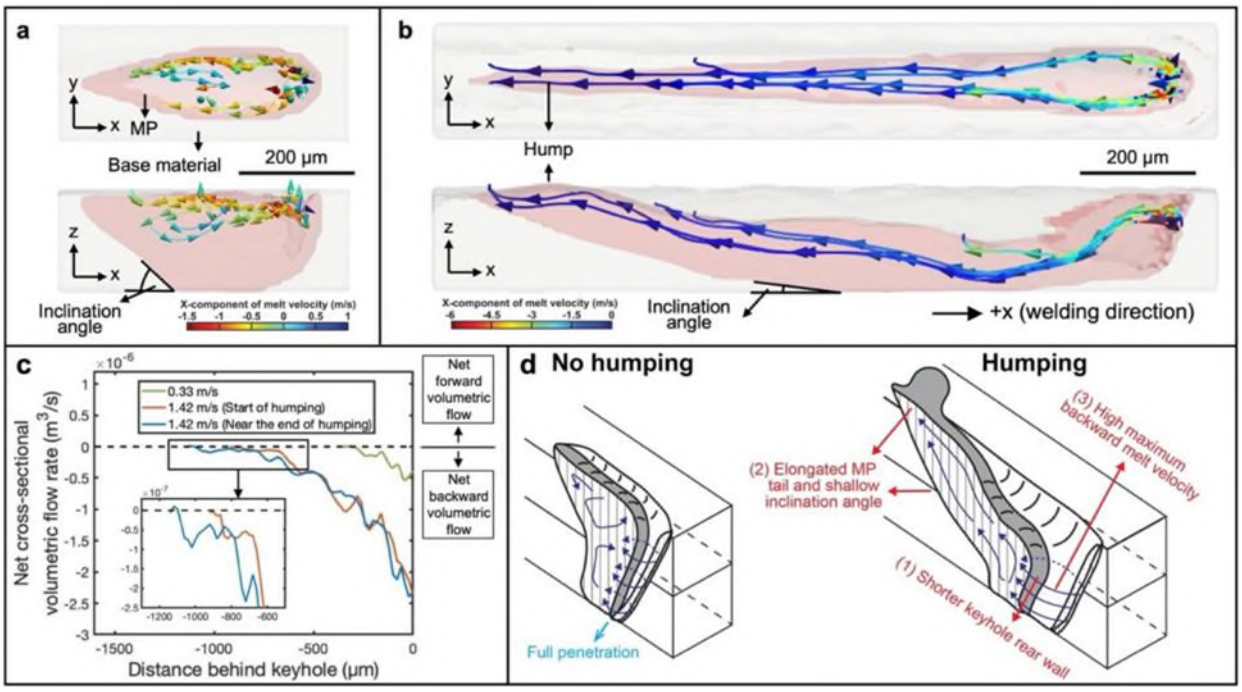

Fig. 4 **a–b** Top and side views of streamlines extracted from CFD simulation results at the welding speeds of 0.33 and 1.42 m/s, respectively. **c** Net cross-sectional volumetric flow rate extracted from different distances of y-z cross-sections behind the keyhole at the welding speeds of 0.33 m/s, 1.42 m/s (start of humping), and 1.42 m/s (near the end of humping), respectively. An enlarged view highlights the curves around the MP tail at 1.42 m/s. **d** Schematic diagram showing the formation mechanisms of humping.

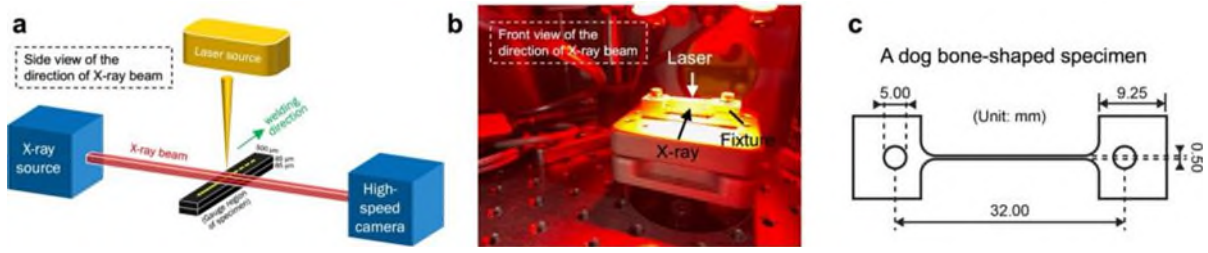

Supplementary Fig. 1 Experimental setup of in situ high-speed synchrotron X-ray imaging at ANL. **a** The side and **b** the front views of the direction of X-ray beam. The laser welding configuration was an overlapped weld. **c** Geometry of the dog bone-shaped specimen. Narrow width (500 μm) in the gauge region is required due to the strong attenuation of X-ray on stainless steel.

C2: In addition, the humping phenomena can also depend on the heat input used. Please include a table comparing the heat input in all cases to help discuss the phenomena.

A2: We appreciate your thoughtful feedback on this matter. The authors agree that heat input plays a crucial role in laser welding. We calculated it using the equation (Heat input $= P \times 11/u_{\&}$ [5]) where P is the power, 11 is the overall welding efficiency (taken as 0.80 from the ref. [6]), and $u_{\&}$ is the laser welding speed. The results are listed in Supplementary Table 1 (Page 30 of the revised manuscript). It shows that when the humping occurs at the welding speeds of 1.00, 1.25, and 1.42 m/s, the corresponding heat inputs are 199.20, 206.72, and 196.06, respectively. The heat inputs in these conditions are slightly lower than those in the other two non-humping conditions. However, even if we increase the heat inputs to match those of the non-humping conditions, humping will still occur at these three welding speeds. Therefore, using heat inputs as a criterion for the onset of humping could be challenging.

Supplementary Table 1 All processing conditions with the corresponding heat inputs calculated by the equation (Heat input $= P \times 11/u_{\&}$ [5]). 11 (overall welding efficiency) is taken as 0.80 from the ref. [6].

Laser welding speed () (m/s)	Power () (W)	Heat input (J/m)
0.33	102	247.27
0.67	188	224.48
1.00*	249	199.20
1.25*	323	206.72
1.42*	348	196.06

*Humping occurred

C3: However, I did not see a detailed discussion about the velocity of fluid flow, the behavior of convection patterns, and the appearance of eddies in the melt pool, especially velocity, in relation to your results. If you have calculated fluid flow velocity, please explain the methods, calibration, and steps used in detail. For guidance, you can refer to the paper: https://iopscience.iop.org/article/10.1088/1361-6463/aa9902/meta. For example, do you use zirconia particles to track the velocity change or any other method? How did you do with it because you did for very thin sheets?

A3: We are grateful for your perceptive and constructive remarks. We attempted to directly observe the melt flow (the velocity of fluid flow, the behavior of convection patterns, and the appearance of eddies in the melt pool) by using W tracer particles in in situ synchrotron X-ray imaging, but the experiments was hard to achieve for the technical limitations, i.e., the thin, narrow sheets and the fine laser spot size (narrow molten pool) used in this study, which was discussed in **A1**. Therefore, we employed CFD simulation to analyze the melt flow velocity and convection

patterns in MP. On the other hand, we are grateful for the reviewer's suggestion to consider zirconia particles. However, we believe it may not be the most effective choice because the density of zirconia (5680 kg/m^3 [7]) is close to that of the molten phase of stainless steel in this study (ranges from 6000 to 7000 kg/m^3, in Supplementary Table 2). A greater density difference is necessary for achieving adequate contrast in synchrotron X-ray imaging. Therefore, zirconia might not be the ideal candidate for tracer particles in this context. Using W particles, with a density of 19250 kg/m^3 [8], is more suitable. However, we have encountered other technical challenges (thin sheet/ narrow MP/ unable to premix powder), as outlined earlier.

Regarding the guidance of describing the methods of melt velocity calculation, we appreciate you providing the link. Unfortunately, we were unable to access it. To enhance the clarity of the analytical approach of the maximum melt velocity $(umax)$ calculation, we have revised the manuscript (Pages 6–7 Lines 136–142):

"In this study, the maximum melt velocity $(umax)$ was calculated by an analytical approach proposed by Beck et al. based on the continuity equation [9] (Equation 1).

$$u_{max} = u_w 1\,1 + [c_p p u_w r \quad 2(c_p(T_m - T_b) + L_m)$$

$$k \quad (1 + \quad c_p(T_b - T_m) \quad)1: \qquad (1)$$

where u_w is the laser welding speed, c_p is the specific heat, p is the density, r is the spot radius, k is the thermal conductivity, and L_m is the latent heat of fusion. T_b, T_m, T_o are the boiling, melting, and room temperatures, respectively. Because u_{max} occurs on the keyhole side wall, as described by Beck et al. [34], the values of c_p, p, and k are obtained at T_b from the thermophysical databases [11,38,39], which is listed in Supplementary Table 2."

Supplementary Table 2 Materials constants used in Equation 1–3 and 5.

Material's constants	Values at T_m	Values at T_b
Density (p)	7000 Tit^3	kgkg 6000 Tit^3
Thermal conductivity (k)	3 30 m•K	45 W m•K
Specific heat (c_p)	I 770 kg•K	I 770 kg•K
Boiling temperature (T_b)	3134 K	
Melting temperature (T?1)	1698 K	
Ambient temperature (T_0)	300 K	
Latent heat of fusion (L*)	2.6×10" I kg	

C4: Maximal melt velocity of 6.0 m/s in Figure 2f needed to provide evidence?

A4: Thank you for your valuable feedback. The maximal melt velocity $(umax)$ of 6.0 m/s was calculated analytically at the welding speed of 1.42 m/s and the power of 348 W. The analytical calculation of u_{max} was performed using an equation derived by Beck et al. [9], as described in

A3. To validate this calculation, we extracted the $_{max}$ from the CFD simulation results, as shown in Fig. L1. $_{max}$ occurs on the keyhole's side wall at 5.69 m/s, closely matching the calculated value of 6.0 m/s from the analytical method. We also extracted $_{max}$ for the 0.33 m/s and 102 W condition, with CFD results consistent with the analytical calculation (Table L1). Therefore, the analytical calculation of $_{max}$ was validated.

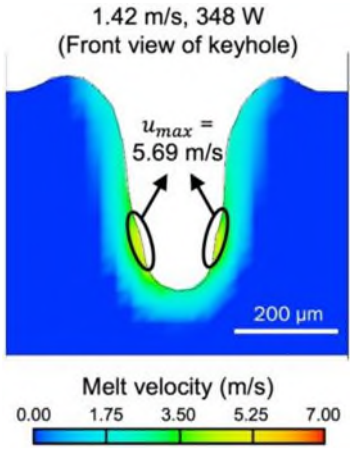

Fig. L1 An example showing the extraction of $_{max}$ from the keyhole side wall in CFD simulation under the welding condition of 1.42 m/s and 348 W.

Table L1 Validation of the calculation of maximum melt velocity (Extracted from Supplementary Table 3)

Condition (Laser welding speed, Laser power)	Key metric	Analytical calculation	Simulation	Error (%)
0.33 m/s, 102 W	Maximum melt velocity (*?@, m/s)	0.86	0.92	7.0
1.42 m/s, 348 W		6.05	5.69	6.0

C5: You mentioned that calculating velocity by experiment is very challenging, and you selected the simulation approaches; it may be OK. But all papers you cited, ref 34, 35, 36, are calculating velocity based on X-rays or other experiments. Therefore, your argument lacks conviction. In addition, ref 35 uses only one X-ray to calculate velocity. Therefore, only 2D images of the melt pool can be revived, and I believe the results may be challenging. Additionally, I don't understand why the humping phenomenon is primarily explained based on CFD results when you have X-ray video data. Discussing the phenomenon based on the X-ray video rather than simulations would be more reliable. You need to include more details based on velocity, convection pattern behavior, and/or the appearance of eddies.
In a recent paper, Anh et al. explained undercut and other defects in the Plasma keyhole welding process based on experiments: https://s3.amazonaws.com/WJ-www.aws.org/supplement/2019.98.018.pdf. You should read this as well. They based their

explanations on X-ray images, velocity calculations, and convection patterns to explain the phenomena of undercut and other defects in detail and reliably. Moreover, I am concerned about your use of only one X-ray source, resulting in 2D projected images of the melt pool, which seems insufficient for calculating the velocity. How do you address this issue?

A5: Thank you for your constructive review and suggestions. We attempted to measure the velocity using W tracer particles in in situ synchrotron X-ray imaging. However, due to technical limitations, we were unsuccessful, as described in **A1**. This approach was successful in refs 34, 35, and 36 mentioned in the manuscript, because of a wider MP or the feasibility of powder premixing. Therefore, in our work, we had to use simulation results. The simulation was validated through several key metrics, including MP dimensions (length, width, depth), the humping phenomenon (linear number density and average hump height), and the maximum melt velocity (′0), as shown in the Supplementary Table 3 below (Page 31 of the revised manuscript). The differences between simulation and experimental measurements are all below 10%, confirming the accuracy of our CFD models.

Supplementary Table 3 Validation of CFD models

Condition	Key metric	Experiment	Simulation	Error (%)
0.33 m/s, 102 W	MP length (j.tm)	368	400	8.7
	MP width (j.tm)	116	120	3.4
	MP depth (j.tm)	170	170	0
	Linear number density of humps (#/mm)	0	0	0
	Average height of humps (j.tm)	N/A	N/A	N/A
	Maximum melt velocity (m/s)	0.86*	0.92	7.0
1.42 m/s, 348 W	MP length (j.tm)	1080	1180	9.3
	MP width (j.tm)	93	100	7.5
	MP depth (j.tm)	170	170	0
	Linear number density of humps (#/mm)	1.50	1.46	2.7
	Average height of humps (j.tm)	58.70 ± 14.82	53.00 ± 15.36	9.7
	Maximum melt velocity (m/s)	6.05*	5.69	6.0

*Obtained from analytical calculation using Equation 1.

Thank you for providing the link to Anh et al.'s work. Unfortunately, we were unable to access it. We made every effort to locate the referenced literature and believe it may correspond to ref. [2]. In their experimental setup, they used two unparallel X-ray beams for three-dimensional observation of the molten pool and melt flow. The results are impressive as they enable spatial analysis of melt flow. However, its application to this study has technical limitations, because separating a synchrotron X-ray beam significantly reduces beam quality and results in substantial energy loss. In this study, our aim was to investigate the humping mechanisms in high-speed laser welding process by leveraging the exceptional properties of synchrotron X-ray imaging, including

its high brightness [10], flux [10], coherency [11], spatial resolution [12], and great penetration depth in stainless steels [10,13]. We chose a side view (2D) for observing the laser welding process, as it offers the best perspective on keyhole and MP dynamics, and humping development. The front view (typically used to observe keyhole formation [14]) and top view (for vapor plume [15] and molten pool width observations [16]) were not the focus of this study.

C6: Additionally, the mechanism of humping formation is not clearly explained in the qualitative analysis.

A6: We sincerely appreciate your thoughtful commentary. To comprehend the mechanisms of humping formation qualitatively, we extracted several key features (depth of keyhole rear wall, MP length, and keyhole width) from the in situ synchrotron X-ray imaging (Fig. 2). As welding speed increased from 0.33 to 1.42 m/s, we observed that the keyhole rear wall shortened, the molten pool lengthened, and the keyhole became more elongated in the welding direction, indicating a higher maximum melt velocity (Fig. 2d–f). These indicated an increase in backward melt velocity and a decrease in the barrier to backward melt flow (shorter keyhole rear wall and shallower inclination angle of the bottom MP boundary) and were therefore identified as the main factors contributing to humping.

The manuscript was revised accordingly to enhance the qualitative discussion on the mechanisms of humping formation (Pages 11–12, Lines 226–236):

“Based on the analyses of in situ high-speed synchrotron X-ray imaging and CFD simulation, the formation mechanisms of humping can be concluded as illustrated in Fig. 4d. First, as the laser welding speed increases, the depth of keyhole rear wall becomes deeper beneath the surface of the base material, reducing the barrier to backward melt flow. Second, the MP length extends with the laser welding speed, failing to decelerate the melt flow effectively and becoming more prone to the Rayleigh instability. Third, the maximum backward melt velocity also rises significantly, increasing the volumetric flow toward the MP tail. These factors enhance backward melt velocity and reduce the flow barrier, leading to greater melt accumulation at the MP tail and triggering humping. When humping occurs, excess melt is released by slightly extending the MP length, which causes the humping to cease temporarily. Therefore, the phenomenon occurs periodically rather than continuously.”

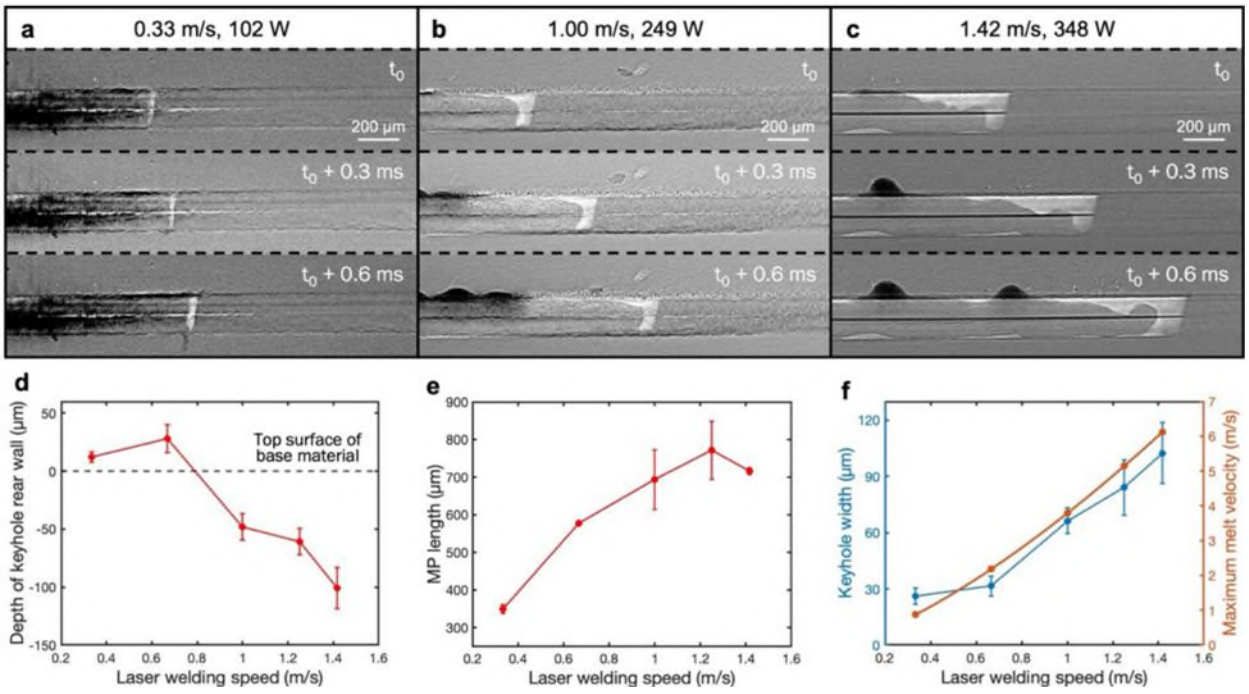

Fig. 2 **a–c** In situ high-speed synchrotron X-ray observations of laser welding at the welding speeds of 0.33, 1.00, and 1.42 m/s at times t_0, t_0 + 0.3, and t_0 + 0.6 ms, where t_0 was arbitrarily selected. See Supplementary Videos 1–5 for in situ observations at five different welding speeds. **d** Depth of keyhole rear wall. **e** MP length. **f** Keyhole width (measured) and maximum melt velocity (max, calculated by Equation 1).

C7: Is your CFD model 2D or 3D? If it is a 3D model, it does not match your experiment, which provides only 2D melt pool images. If you are using CFD models to estimate the humping phenomenon, can you perform experiments under the same conditions as the CFD models to validate your simulation theory?

A7: Thank you for your perceptive and constructive remarks. Both the CFD simulations and laser welding experiments were conducted in 3D under the same process conditions (spot radius, laser welding speed, laser power, sample geometry and configuration). In this study, we only observed the laser welding process from a 2D side view using synchrotron X-ray imaging because separation of synchrotron X-ray into two unparallel beams would significantly reduce the beam quality, as discussed in **A4**. The side view was chosen because it can provide us key information on keyhole and MP dynamics as well as the humping phenomenon. On the other hand, the CFD simulations were validated using multiple key metrics such as MP dimensions, humping characteristics, and maximum melt velocity to ensure the simulation accuracy, as described in **A4**.

C8: In Figure 5, you clearly showed the boundary of humping and no humping by simulation. However, it is better if you can re-do the experiments to validate these simulation estimations.

A8: Thank you for your valuable feedback. Fig. 5 presents the development of the dimensionless humping index (η_{th}) and the boundary between humping and no humping (process window) defined by this index. We would like to clarify that the η_{th} was calculated analytically based on MP characteristics (maximum melt velocity and MP length) and material constants (density, specific heat, thermal conductivity, and surface tension) rather than through simulation. The maximum melt velocity was calculated by an analytical equation derived by Beck et al. [9]. More details can be found in **A3**. The MP length was fitted with process parameters using the data from this study and other literatures [17,18] (Fig. 5a). The materials constants were extracted from literatures [19–21]. We then calculated η_{th} using the process conditions in this study and other literatures [17,22,23], as shown in Fig. 5b. We observed that humping only occurred when η_{th} was greater than 10,000. Therefore, the boundary between humping and no humping (onset threshold

of humping) is set to η_{th} = 10,000. The detailed calculations are summarized in an Excel sheet, along with the submission. It can also be accessed by using the following link (https://docs.google.com/spreadsheets/d/1Qme_ugVUo20zT-H6THDmkeARzsbg8PD7/edit?usp=share_link&ouid=106704118552394079030&rtpof=true&sd=true). After capturing the onset threshold of humping, we calculated the contour plots using spot radii () of 50 and 25 tm, as shown in Fig. 5c–d. On the other hand, it is noted that Fig. 5c–d includes isolines for various weld penetration depths, calculated based on the scaling law from references [23,24]. The isolines provide guidelines for the required power of each penetration depth. The intersection of each penetration depth isoline with the η_{th} of 10,000 defines the laser welding speed and power for the onset of humping.

To further validate this analytical approach, we added an additional set of laser welding condition using a spot radius () of 13 tm alongside the previous case (= 21.5 tm) to confirm the onset threshold of humping (η_{th} of 10,000) in Supplementary Fig. 5 (Page 29 of the revised manuscript). In this figure, the green region indicates no humping, while the red region signifies where humping occurs. Circles and triangles denote experimental results without and with humping, respectively. The black line represents a 170 tm penetration depth, equal to the total thickness of the two overlapping stainless steel foils in this study. It can be observed that all experimental data points (circles and triangles) align with the humping predictions from this study and closely follows the calculated 170 tm penetration depth isoline. Therefore, the onset threshold for humping has been further validated.

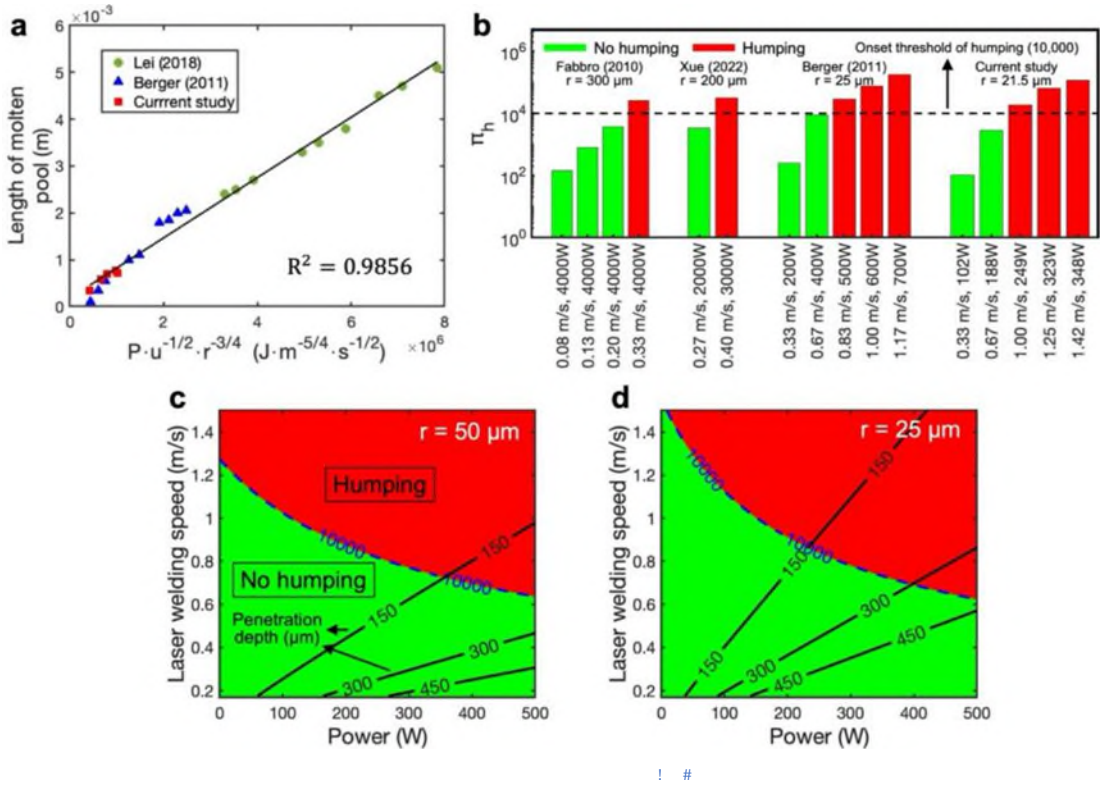

Fig. 5 **a** Scaling law between the MP length and $P/\sqrt{v}r^{3/4}$ (R^2 =0.9856) performed using the experimental results from the current study and other literatures [8,44]. **b** Calculated dimensionless humping index π_h. The onset threshold occurs at approximately 10,000 across different published data [8,9,22]. **c–d** Process windows with (red) and without humping (green) separated by the 10,000-isoline of π_h and penetration depth (p_m) calculated by scaling law [22,43] at the spot radii (r) of 50 and 25 μm.

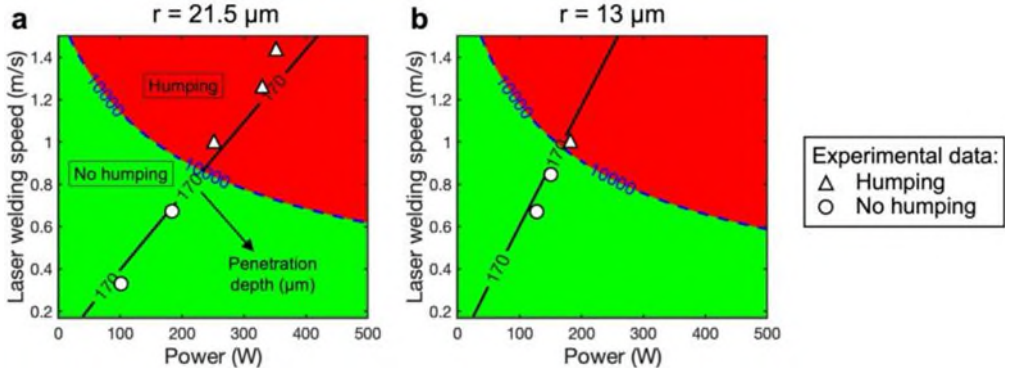

Supplementary Fig. 5 Experimental results along with the onset threshold of humping (π_h of 10,000) and the isoline of penetration depth of 170 μm for spot radii of **a** 21.5 μm and **b** 13 μm.

The process windows in Fig. 5c–d suggest several strategies to increase the laser welding speed without humping, which is the engineering goal for this research. The first approach is to employ

a finer spot radius (). For example, the critical laser welding speed increases from 0.72 to 0.87 m/s at a penetration depth of 150 tm when is reduced from 50 to 25 tm (Fig. 5c–d). The second method is to reduce the thickness of the base material, which means a smaller penetration depth. For instance, the critical welding speed increases from 0.68 to 0.87 m/s at =25 tm when the thickness is reduced from 300 to 150 tm (Fig. 5d).

C9: Previous studies have investigated the humping phenomenon using high-speed optical cameras [6–8] or X-ray imaging equipment with a lower frame rate (e.g., 1000 fps in [4]) compared to the 20,000 fps synchrotron X-ray imaging we used. For laser welding, 20,000 fps is still low due to the speed of the laser spot, but for plasma welding, 1000 fps is sufficient for calculations with proper calibration and literature-based discussion. The number of frames used depends on the specific process.

A9: We sincerely appreciate your thoughtful commentary. The authors agree that the required temporal resolution (frame rate) depends on the specific processes and parameters involved. A temporal resolution of 1000 ts (1000 fps) was sufficient for plasma welding, as reported in study [2]. In our study, the temporal resolution was 50 ts (20,000 fps). We also reviewed the temporal resolutions used in other studies on in situ observations of laser welding and additive manufacturing, as summarized in the table below. The temporal resolution employed in this study is comparable to those. Additionally, the camera's exposure time was 1 ts. For example, at the fastest welding speed (1.42 m/s), the keyhole moved only 1.42 tm during this exposure, which was smaller than the camera's pixel size (2 tm). Thus, the exposure time of camera was sufficient to capture the instantaneous geometries and movements of the keyhole and MP.

Ref.	Process	Laser moving or welding speeds (m/s)	Temporal resolution (j.ts)	Exposure time of camera (j.ts)
Chen et al. (2020) [25]	Laser powder bed fusion	0.1	Not provided	12.5
Gan et al. (2021) [26]	Laser powder bed fusion	0.3–1.2	20–50	1–40
Schricker et al.(2022) [27]	Laser welding	0.16	50	Not provided
Our study	Laser welding	0.33–1.42	50	1

C10: In some figures, the scale bar and number are not clear or not mentioned.

A10: Thank you for your comment. We initially followed the journal's guideline, which states: "Scale bars should be used rather than magnification factors, with the length of the bar defined in the legend rather than on the bar itself" (https://www.nature.com/ncomms/submit/how-to-submit). However, we have recently observed that some papers published in *Nature Communications*

include scale bars with the length defined directly on the bar itself, indicating that both approaches are acceptable. We have revised the figures and supplementary videos to include the length directly on the bar, as shown below.

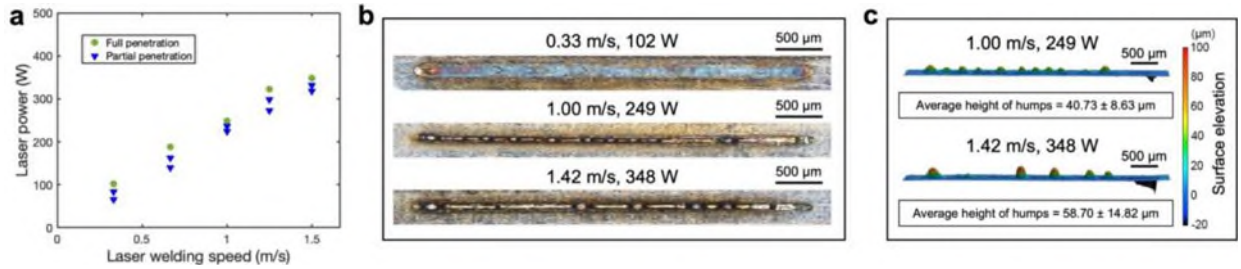

Fig. 1 **a** The corresponding laser power at each welding speed was determined at EWI by incrementally increasing the laser power until full penetration was achieved. **b** Top surfaces of weld seams at the welding speeds of 0.33, 1.00, and 1.42 m/s. Note that the fastest speed was adopted as 1.42 m/s instead of 1.50 m/s due to the equipment setup at ANL. **c** Surface topography of weld seams at 1.00 and 1.42 m/s, and the average hump height relative to the weld top surface.

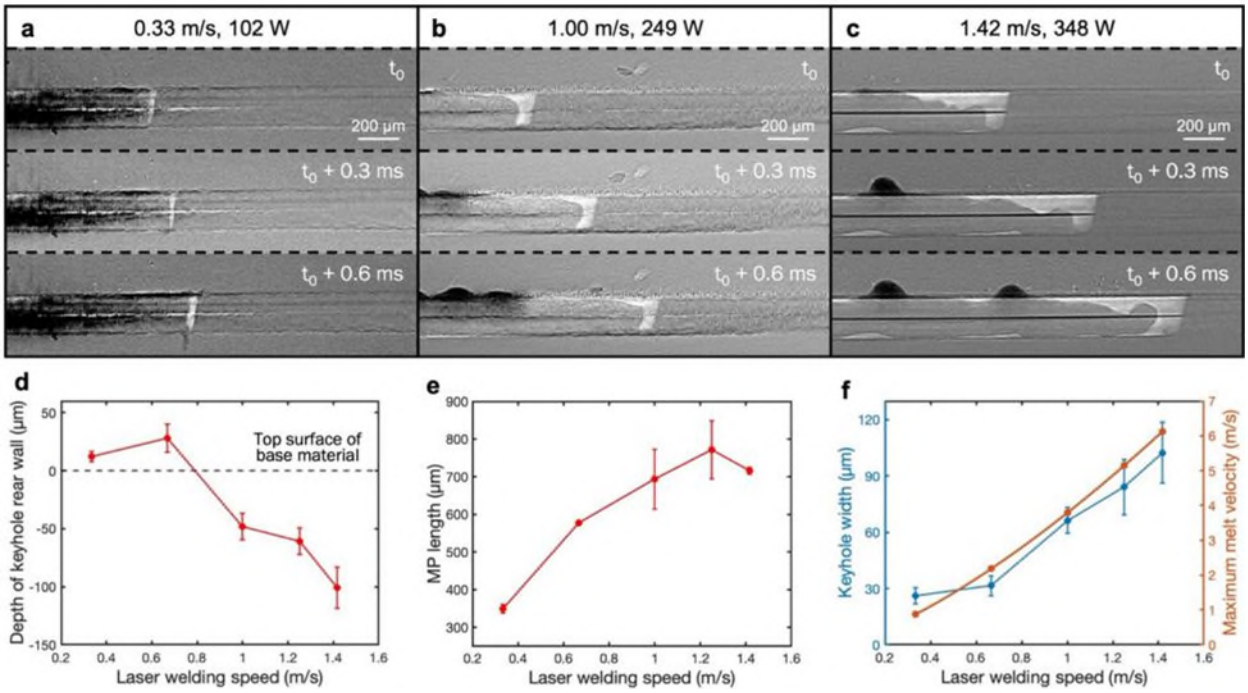

Fig. 2 **a–c** In situ high-speed synchrotron X-ray observations of laser welding at the welding speeds of 0.33, 1.00, and 1.42 m/s at times t_0, t_0 + 0.3, and t_0 + 0.6 ms, where t_0 was arbitrarily selected. See Supplementary Videos 1–5 for in situ observations at five different welding speeds. **d** Depth of keyhole rear wall. **e** MP length. **f** Keyhole width (measured) and maximum melt velocity (max, calculated by Equation 1).

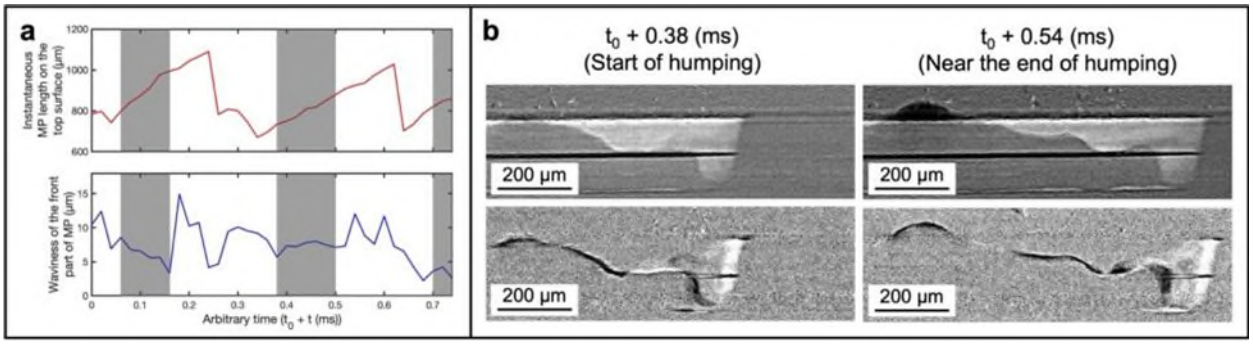

Fig. 3 Analysis of humping cycle at the welding speed of 1.42 m/s. **a** MP length on the top surface and waviness of the front part of MP, with the starting periods of humping marked in grey. **b** Examples of MP waviness changes during humping. At the start of humping ($_0$ + 0.38 ms), the average MP waviness was lower. Near an end ($_0$ + 0.54 ms), the MP surface showed higher waviness because of the steeper gradient of the backward melt flow's volumetric rate.

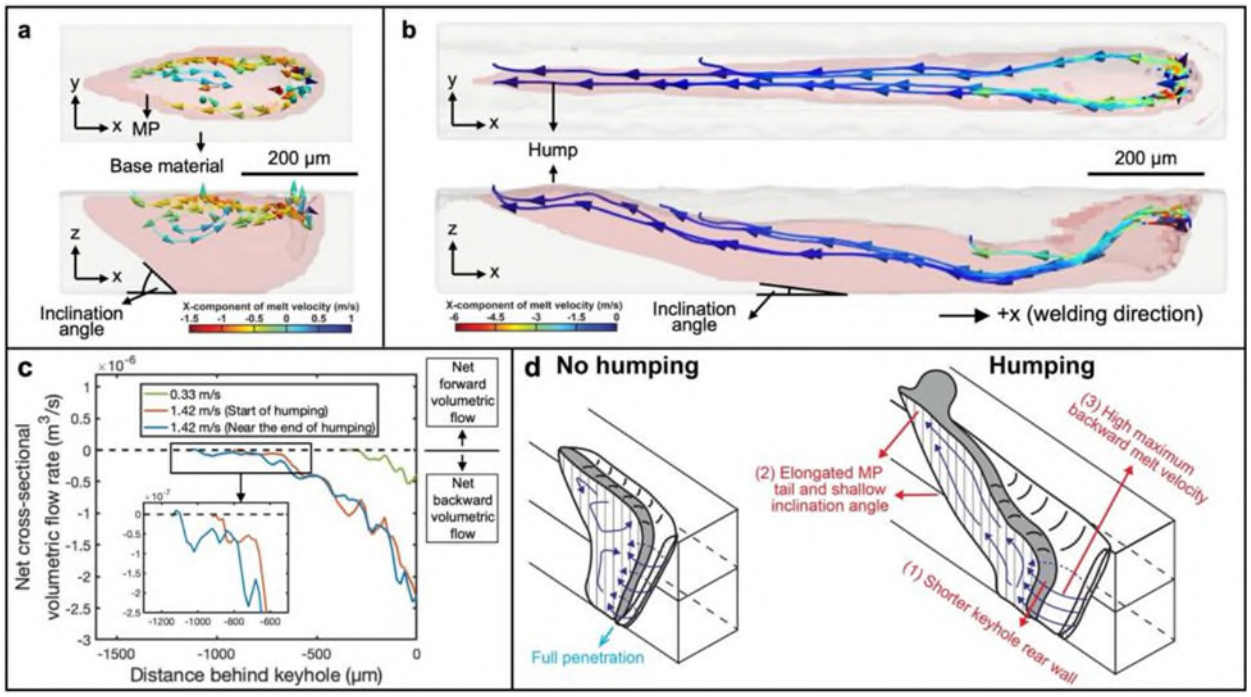

Fig. 4 **a–b** Top and side views of streamlines extracted from CFD simulation results at the welding speeds of 0.33 and 1.42 m/s, respectively. **c** Net cross-sectional volumetric flow rate extracted from different distances of y-z cross-sections behind the keyhole at the welding speeds of 0.33 m/s, 1.42 m/s (start of humping), and 1.42 m/s (near the end of humping), respectively. An enlarged view highlights the curves around the MP tail at 1.42 m/s. **d** Schematic diagram showing the formation mechanisms of humping.

Reviewer #2

C1: Overall, the authors have answered most questions I raised. Please also comment about the dissimilar bonding by using this possible future modification in modeling and it is not mandatory. Yes, it is worthy to be published in this Journal.

A1: Thank you for your comment. Flow3D can handle CFD simulation of laser welding provided that the temperature-dependent physical properties and absorption rates of both base materials are available.

References

[1] L. Aucott, H. Dong, W. Mirihanage, R. Atwood, A. Kidess, S. Gao, S. Wen, J. Marsden, S. Feng, M. Tong, T. Connolley, M. Drakopoulos, C.R. Kleijn, I.M. Richardson, D.J. Browne, R.H. Mathiesen, Helen. V Atkinson, Revealing internal flow behaviour in arc welding and additive manufacturing of metals, Nat Commun 9 (2018) 5414. https://doi.org/10.1038/s41467-018-07900-9.

[2] A. Van Nguyen, S. Tashiro, M.H. Ngo, H. Van Bui, M. Tanaka, Effect of the eddies formed inside a weld pool on welding defects during plasma keyhole arc welding, J Manuf Process 59 (2020) 649–657. https://doi.org/https://doi.org/10.1016/j.jmapro.2020.10.020.

[3] Q. Guo, M. Qu, L.I. Escano, S.M.H. Hojjatzadeh, Z. Young, K. Fezzaa, L. Chen, Revealing melt flow instabilities in laser powder bed fusion additive manufacturing of aluminum alloy via in-situ high-speed X-ray imaging, Int J Mach Tools Manuf 175 (2022) 103861. https://doi.org/https://doi.org/10.1016/j.ijmachtools.2022.103861.

[4] S.M.H. Hojjatzadeh, N.D. Parab, W. Yan, Q. Guo, L. Xiong, C. Zhao, M. Qu, L.I. Escano, X. Xiao, K. Fezzaa, W. Everhart, T. Sun, L. Chen, Pore elimination mechanisms during 3D printing of metals, Nat Commun 10 (2019) 3088. https://doi.org/10.1038/s41467-019-10973-9.

[5] K.Y. Benyounis, A.G. Olabi, M.S.J. Hashmi, Effect of laser welding parameters on the heat input and weld-bead profile, J Mater Process Technol 164–165 (2005) 978–985. https://doi.org/https://doi.org/10.1016/j.jmatprotec.2005.02.060.

[6] P.W. Fuerschbach, Measurement and prediction of energy transfer efficiency in laser beam welding, 75 (1996). https://doi.org/doi:10.1107/S0909049506000550.

[7] Zirconium dioxide, (n.d.). https://en.wikipedia.org/wiki/Zirconium_dioxide.

[8] Tungsten, (n.d.). https://en.wikipedia.org/wiki/Tungsten.

[9] M. Beck, P. Berger, F. Dausinger, H. Huegel, Aspects of keyhole/melt interaction in high-speed laser welding, in: Proc.SPIE, 1991: pp. 769–774. https://doi.org/10.1117/12.25985.

[10] G.K. Shenoy, Impact of next-generation synchrotron radiation sources on materials research, Nucl Instrum Methods Phys Res B 199 (2003) 1–9. https://doi.org/https://doi.org/10.1016/S0168-583X(02)01594-X.

[11] D.H. Bilderback, P. Elleaume, E. Weckert, Review of third and next generation synchrotron light sources, Journal of Physics B: Atomic, Molecular and Optical Physics 38 (2005) S773. https://doi.org/10.1088/0953-4075/38/9/022.

[12] T. Martin, A. Koch, Recent developments in X-ray imaging with micrometer spatial resolution, J Synchrotron Radiat 13 (2006) 180–194. doi:10.1107/S0909049506000550 (accessed August 19, 2024).

[13] L. Mino, E. Borfecchia, J. Segura-Ruiz, C. Giannini, G. Martinez-Criado, C. Lamberti, Materials characterization by synchrotron x-ray microprobes and nanoprobes, Rev Mod Phys 90 (2018) 25007. https://doi.org/10.1103/RevModPhys.90.025007.

[14] R. Cunningham, C. Zhao, N. Parab, C. Kantzos, J. Pauza, K. Fezzaa, T. Sun, A.D. Rollett, Keyhole threshold and morphology in laser melting revealed by ultrahigh-speed x-ray imaging, Science (1979) 363 (2019) 849–852. https://doi.org/10.1126/science.aav4687.

[15] B. Xue, B. Chang, D. Du, Monitoring of high-speed laser welding process based on vapor plume, Opt Laser Technol 147 (2022) 107649. https://doi.org/https://doi.org/10.1016/j.optlastec.2021.107649.

[16] T.-N. Le, M.-H. Lee, Z.-H. Lin, H.-C. Tran, Y.-L. Lo, Vision-based in-situ monitoring system for melt-pool detection in laser powder bed fusion process, J Manuf Process 68 (2021) 1735–1745. https://doi.org/https://doi.org/10.1016/j.jmapro.2021.07.007.

[17] P. Berger, H. Hügel, A. Hess, R. Weber, T. Graf, Understanding of Humping Based on Conservation of Volume Flow, Phys Procedia 12 (2011) 232–240. https://doi.org/10.1016/j.phpro.2011.03.030.

[18] T. Lei, Y. Rong, J. Xu, Y. Huang, Experiment study and regression analysis of molten pool in laser welding, Opt Laser Technol 108 (2018) 534–541. https://doi.org/https://doi.org/10.1016/j.optlastec.2018.07.053.

[19] X. Meng, G. Qin, Z. Zou, Investigation of humping defect in high speed gas tungsten arc welding by numerical modelling, Mater Des 94 (2016) 69–78. https://doi.org/https://doi.org/10.1016/j.matdes.2016.01.019.

[20] N. Chen, H.A. Khan, Z. Wan, J. Lippert, H. Sun, S.-L. Shang, Z.-K. Liu, J. Li, Microstructural characteristics and crack formation in additively manufactured bimetal material of 316L stainless steel and Inconel 625, Addit Manuf 32 (2020) 101037. https://doi.org/https://doi.org/10.1016/j.addma.2020.101037.

[21] C.S. Kim, Thermophysical properties of stainless steels, United States, 1975. https://doi.org/10.2172/4152287.

[22] B. Xue, B. Chang, S. Wang, R. Hou, P. Wen, D. Du, Humping Formation and Suppression in High-Speed Laser Welding, Materials 15 (2022). https://doi.org/10.3390/ma15072420.

[23] R. Fabbro, Melt pool and keyhole behaviour analysis for deep penetration laser welding, J Phys D Appl Phys 43 (2010) 445501. https://doi.org/10.1088/0022-3727/43/44/445501.

[24] A.M. Rubenchik, W.E. King, S.S. Wu, Scaling laws for the additive manufacturing, J Mater Process Technol 257 (2018) 234–243. https://doi.org/https://doi.org/10.1016/j.jmatprotec.2018.02.034.

[25] Y. Chen, S.J. Clark, C.L.A. Leung, L. Sinclair, S. Marussi, M.P. Olbinado, E. Boller, A. Rack, I. Todd, P.D. Lee, In-situ Synchrotron imaging of keyhole mode multi-layer laser powder bed fusion additive manufacturing, Appl Mater Today 20 (2020) 100650. https://doi.org/https://doi.org/10.1016/j.apmt.2020.100650.

[26] Z. Gan, O.L. Kafka, N. Parab, C. Zhao, L. Fang, O. Heinonen, T. Sun, W.K. Liu, Universal scaling laws of keyhole stability and porosity in 3D printing of metals, Nat Commun 12 (2021) 2379. https://doi.org/10.1038/s41467-021-22704-0.

[27] K. Schricker, L. Schmidt, H. Friedmann, C. Diegel, M. Seibold, P. Hellwig, F. Fröhlich, J.P. Bergmann, F. Nagel, P. Kallage, A. Rack, H. Requardt, Y. Chen, Characterization of keyhole dynamics in laser welding of copper by means of high-speed synchrotron X-ray imaging, Procedia CIRP 111 (2022) 501–506. https://doi.org/https://doi.org/10.1016/j.procir.2022.08.079.

Response Letter

Reviewer #1

Thank you for your effort in revising the manuscript. You've addressed most of my questions, and I'm satisfied with your responses. However, I have a few comments where it seems there may have been some misunderstandings.

C1: For instance, in Table 3, you compare experimental and simulation results, but it's unclear how and where you obtained the experimental data. Did you conduct the experiments yourself, or were the results cited from other papers? If the data was cited from other papers, please verify that the source/paper used two X-ray sources, as the use of only one X-ray source would result in 2D images and videos, which could lead to incorrect velocity measurements. If the data was from other groups, please ensure you are citing studies that used two X-ray sources. If the experiment was conducted by your team, how was the velocity measured?

A1: We appreciate the reviewer's thoughtful comments. In Supplementary Table 3 of NCOMMS-24-15270B (submitted on Sep 6th, 2024), we compared the maximum melt velocity (u_{max}) obtained from analytical calculations using Equation 1 (Beck et al. [1]) with the results from computational fluid dynamics (CFD) simulations. However, we did not obtain u_{max} in our in situ synchrotron X-ray imaging experiments.

We would like to clarify that we conducted the in situ synchrotron X-ray imaging experiments to investigate keyhole and molten pool dynamics. However, we did not directly measure u_{max} in these experiments, as we could not add tracer particles (e.g., W particles with a diameter of 10–20 μm), which were too large compared to the molten pool width (80–100 μm) to accurately measure the melt flow velocity. Therefore, we relied on the analytical approach (Equation 1, derived by Beck et al. [1]) to calculate u_{max}.

$$u_{max} = u_w \left\{ 1 + \left[\frac{c_p \rho u_w r}{k} \left(1 + \frac{2\left(c_p (T_m - T_0) + L_m\right)}{c_p (T_b - T_m)} \right) \right]^{0.5} \right\} \quad (1)$$

The description for each notation in Equation 1 is provided in Table L1, where c_p, ρ, k, L_m, T_b, and T_m are material's constants obtained from databases [2–4], T_0 is the room temperature, and u_w (laser welding speed) and r (laser spot radius) are laser process variables used in our experiments, as listed in Table L2. The analytical calculations were consistent with the results from our CFD simulations, as shown in Supplementary Table 4.

Table L1 Description of each notation in Equation 1 and the corresponding values.

Notation	Description	Data source	Value (Unit)
c_p	Specific heat	Material's constants obtained from the databases [2–4]	$770\,\frac{J}{kg \cdot K}$
ρ	Density		$6000\,\frac{kg}{m^3}$
k	Thermal conductivity		$45\,\frac{W}{m \cdot K}$
L_m	Latent heat of fusion		$2.6\times10^5\,\frac{J}{kg}$
T_b	Boiling temperature		$3134\,K$
T_m	Melting temperature		$1698\,K$
T_0	Toom temperature		$300\,K$
u_w	Laser welding speed	Experimental process parameters of our work	See Table L2
r	Laser spot radius		

Table L2 Laser welding process parameters used in this work.

Laser spot radius (r, m)	Laser welding speed (u_w, m/s)
2.15×10^{-5}	0.33
	0.67
	1.00
	1.25
	1.42

In the last revision (NCOMMS-24-15270B), we marked the analytical calculations of u_{max} as "*Obtained from analytical calculation using Equation 1" under the "experiment" column in Supplementary Table 3. In this revised manuscript, we split this table into Supplementary Tables 3 and 4 for clarity. Table 3 now presents experimental values compared to CFD simulation results, and Table 4 lists analytical calculations against CFD results. Our CFD simulations, validated by three MP dimensions, linear humping number density, and average height (all errors are below 10%, Supplementary Table 3), show good agreement with the analytical u_{max} values (Supplementary Table 4). Both tables are on page 31 of the revised manuscript, and the updated text is from lines 397–402 on page 20.

Supplementary Table 3 Validation of CFD simulation models, including MP dimensions (length, width, depth) and humping characteristics (linear number density and average height of humps).

Condition	Feature	Experiment	CFD simulation	Error (%)
0.33 m/s, 102 W	MP length (µm)	368*	400	8.7
	MP width (µm)	116^	120	3.4
	MP depth (µm)	170*	170	0
1.42 m/s, 348 W	MP length (µm)	1080*	1180	9.3
	MP width (µm)	93^	100	7.5
	MP depth (µm)	170*	170	0
	Linear number density of humps (#/mm)	1.50^	1.46	2.7
	Average height of humps (µm)	58.70 ± 14.82^	53.00 ± 15.36	9.7

* From in situ synchrotron X-ray imaging of laser welding process

^ From optical profilometry of the top surfaces of laser welds

Supplementary Table 4 The maximum melt velocity (u_{max}) from analytical calculations using Equation 1 (Beck et al. [1]) and CFD simulations.

Condition	Feature	Analytical calculation	CFD simulation	Error (%)
0.33 m/s, 102 W	Maximum melt velocity (u_{max}, m/s)	0.86	0.92	7.0
1.42 m/s, 348 W		6.05	5.69	6.0

We also appreciate the reviewer for pointing out the confusions regarding references [5–7]. We did not use data from these references, which used 2D X-ray observations with tracer particles to visualize the melt flow and to measure the 2D projected melt velocity. We agree that the calculated velocity in these references may be inaccurate due to the lack of 3D considerations. We have revised the manuscript accordingly (Page 6, Lines 132–138):

"In terms of melt flow velocity measurement, literatures reported adding W or Ta tracer particles during in situ X-ray experiments [34–36]. However, this approach is limited by the particle size relative to the MP dimensions and the feasibility of materials premixing. This approach has been applied in arc welding [34] for its larger MP size and powder bed fusion [35,36] where tracer particles were premixed with the powder bed. These experiments provided direct melt flow observations, and it should be noted that the velocity measurements were restricted to two dimensions, as only 2D projected images were used."

C2: A velocity of 6 m/s seems unusually high, and it might be unrealistic. It would be beneficial to discuss this value in the context of previously published papers. For example, I have read papers by Prof. Katayama on laser welding, and his measured velocities don't seem to reach 6 m/s. Please make sure this is addressed properly. As for Comment C5, please refer to the paper I provided. I

apologize if there were any difficulties in accessing it. Title paper: Undercut Formation Mechanism in Keyhole Plasma Arc Welding Link: https://s3.amazonaws.com/WJ-www.aws.org/supplement/2019.98.018.pdf

A2: We are grateful for the reviewer's insightful comment. We compare our analytical calculations of maximum melt velocity (u_{max}) with the calculation or 3D CFD simulation reported from other literatures [1,8], as shown in Table L3. It is noted that because we could not find literatures reporting u_{max} for laser welding using a welding speed (u_w) close to our study (1.42 m/s), we included Tang et al.'s study on laser powder bed fusion [8] for comparison of u_{max}. It can be observed that u_{max} range from 3.75–9.00 m/s when the u_w or the laser scanning speed ranges from 1.00–1.60 m/s for these studies. It is also noted that differences in material's constants (Table L4) can cause a slight difference in u_{max}, as seen when comparing our results (for stainless steel) with Beck et al.'s calculation result [1] (for pure Fe). Based on the above discussions, we believe that our u_{max} calculations are reasonable and realistic.

Table L3 Maximum melt velocity (u_{max}) calculated from this study and reported from other literatures [1,8].

Reference	Material	Laser welding speed (u_w) or scanning speed (m/s)	Maximum melt velocity (u_{max}, m/s)	Approach to obtain u_{max}
Beck et al. [1]	Pure Fe	1.00	5.50	Analytical calculation using Equation 1
Current study	Stainless steel	1.00	3.75	
Current study	Stainless steel	1.42	6.05	
Tang et al. [8]	Stainless steel	1.60*	~9.00	3D CFD simulation

* Represents the laser scanning speed in laser powder bed fusion process

Table L4 Materials constants of stainless steels [2–4] and pure Fe [1] used for u_{max} calculation.

Material's constants	Stainless steels	Pure Fe
Density (ρ)	$6000\,\frac{kg}{m^3}$	$7800\,\frac{kg}{m^3}$
Thermal conductivity (k)	$45\,\frac{W}{m\cdot K}$	$42.5\,\frac{W}{m\cdot K}$
Specific heat (c_p)	$770\,\frac{J}{kg\cdot K}$	$796.2\,\frac{J}{kg\cdot K}$
Boiling temperature (T_b)	$3134\,K$	$3000\,K$
Melting temperature (T_m)	$1698\,K$	$1812\,K$
Ambient temperature (T_0)	$300\,K$	$300\,K$
Latent heat of fusion (L_m)	$2.6\times10^5\,\frac{J}{kg}$	$2.6\times10^5\,\frac{J}{kg}$

We thank the reviewer for mentioning Prof. Katayama's literature, which we believe refers to reference [9]. We also appreciate the reviewer for directing us to Prof. Tanaka's work [10]. Table L5 compares u_w and u_{max} from these two studies with our work. The analytical calculation of u_{max} from our work is reasonable when compared to both references [9,10]. According to Equation 1, u_{max} is positively correlated with u_w, so Prof. Katayama's work [9] reported a lower

u_{max} (u_{max} = 0.40–0.89 m/s at u_w = 0.10–0.15 m/s) compared to our work (u_{max}= 6.05 m/s at u_w=1.42 m/s), as shown in Table L5. The $\frac{u_{max}}{u_w}$ ratio in our study (4.26) also falls within the range reported by Prof. Katayama (4.00–5.93 [9]). These discussions further support the validity and realism of our u_{max} calculation.

Regarding Prof. Tanaka's work [10] on plasma arc welding, because of its lower welding speed (0.003 m/s), the resulting u_{max} (0.32–1.3 m/s depending on the plasma gas flow rate) is lower than the u_{max} (6.05 m/s) when u_w is 1.42 m/s in our study, as presented in Table L5. It is noted that because plasma arc welding is a different process, u_{max} may not fully follow Equation 1.

Table L5 Comparison of maximum melt velocity (u_{max}) between this study, Prof. Katayama's work [9], and Prof. Tanaka's work [10].

Reference	Process	Laser welding speed (u_w, m/s)	Maximum melt velocity (u_{max}, m/s)	$\frac{u_{max}}{u_w}$	Approach to obtain u_{max}
Katayama et al. [9]	Laser welding	0.10	0.40	4.00	3D X-ray imaging
		0.15	0.89	5.93	
Current study	Laser welding	1.42	6.05	4.26	Analytical calculation using Equation 1
Tanaka et al. [10]	Plasma arc welding	0.003	0.32–1.3	A different process	3D X-ray imaging

References

[1] M. Beck, P. Berger, F. Dausinger, H. Huegel, Aspects of keyhole/melt interaction in high-speed laser welding, in: Proc.SPIE, 1991: pp. 769–774. https://doi.org/10.1117/12.25985.

[2] X. Meng, G. Qin, Z. Zou, Investigation of humping defect in high speed gas tungsten arc welding by numerical modelling, Mater Des 94 (2016) 69–78. https://doi.org/https://doi.org/10.1016/j.matdes.2016.01.019.

[3] N. Chen, H.A. Khan, Z. Wan, J. Lippert, H. Sun, S.-L. Shang, Z.-K. Liu, J. Li, Microstructural characteristics and crack formation in additively manufactured bimetal material of 316L stainless steel and Inconel 625, Addit Manuf 32 (2020) 101037. https://doi.org/10.1016/j.addma.2020.101037.

[4] C.S. Kim, Thermophysical properties of stainless steels, United States, 1975. https://doi.org/10.2172/4152287.

[5] L. Aucott, H. Dong, W. Mirihanage, R. Atwood, A. Kidess, S. Gao, S. Wen, J. Marsden, S. Feng, M. Tong, T. Connolley, M. Drakopoulos, C.R. Kleijn, I.M. Richardson, D.J. Browne, R.H. Mathiesen, Helen. V Atkinson, Revealing internal flow behaviour in arc welding and

additive manufacturing of metals, Nat Commun 9 (2018) 5414. https://doi.org/10.1038/s41467-018-07900-9.

[6] Q. Guo, M. Qu, L.I. Escano, S.M.H. Hojjatzadeh, Z. Young, K. Fezzaa, L. Chen, Revealing melt flow instabilities in laser powder bed fusion additive manufacturing of aluminum alloy via in-situ high-speed X-ray imaging, Int J Mach Tools Manuf 175 (2022) 103861. https://doi.org/https://doi.org/10.1016/j.ijmachtools.2022.103861.

[7] S.M.H. Hojjatzadeh, N.D. Parab, W. Yan, Q. Guo, L. Xiong, C. Zhao, M. Qu, L.I. Escano, X. Xiao, K. Fezzaa, W. Everhart, T. Sun, L. Chen, Pore elimination mechanisms during 3D printing of metals, Nat Commun 10 (2019) 3088. https://doi.org/10.1038/s41467-019-10973-9.

[8] C. Tang, K.Q. Le, C.H. Wong, Physics of humping formation in laser powder bed fusion, Int J Heat Mass Transf 149 (2020) 119172. https://doi.org/https://doi.org/10.1016/j.ijheatmasstransfer.2019.119172.

[9] Y. Kawahito, Y. Uemura, Y. Doi, M. Mizutani, K. Nishimoto, H. Kawakami, M. Tanaka, H. Fujii, K. Nakata, S. Katayama, Elucidation of the effect of welding speed on melt flows in high-brightness and high-power laser welding of stainless steel on basis of three-dimensional X-ray transmission in situ observation, Welding International 31 (2017) 206–213. https://doi.org/10.1080/09507116.2016.1223204.

[10] A. V Nguyen, D. Wu, S. Tashiro, M. Tanaka, Undercut formation mechanism in keyhole plasma arc welding, Weld J 98 (2019) 204–212.

Response Letter

Reviewer #1

C1: Thank you for your reply. I'm okay with most of your response. However, I find the additional sentences you included in the manuscript unclear. I believe it's widely understood that using a single X-ray source from a side view can only produce 2D projected images and videos, making it impossible to calculate velocity within the melt pool. I agree that you should clearly state that using one X-ray source, as referenced in the published papers, makes velocity calculation impossible. As you mentioned, the term "projected velocity" doesn't apply here. It is impossible to calculate velocity without sufficient data from the X, Y, and Z axes. Therefore, I suggest you explicitly mention in your paper that calculating the flow velocity in the melt pool with just one X-ray source is not feasible. Additionally, the melt pool is extremely small, making it highly challenging to use W or Ta particles, which is why you opted to use the CFD model. In fact, the issue with a small melt pool is just one aspect of the challenge. The core issue, as in references 34–36 and in your paper, is that it's impossible to calculate velocity with a single X-ray source, so using a CFD model to make predictions is a reasonable approach. Please consider this and your paper can be published.

A1: We appreciate the reviewer's thoughtful comments. We agree that it can be inaccurate to calculate the melt velocity by using only 2-dimensional (2D) projected images because it did not consider the three-dimensional (3D) melt flow. We have revised the manuscript to emphasize this point (Page 7 Lines 140–142):

"It should be noted that quantitative velocity measurements using a single X-ray source from a side view, producing 2D images, may be inaccurate as they may not fully capture the complexities of 3D flow dynamics."

Although this approach was used in references [1–3], our study utilized computational fluid dynamics (CFD) simulations to analyze melt flow velocity. Our 3D CFD model overcomes the limitations of 2D projections. We have updated the manuscript to highlight this point (Page 10 Lines 203–204):

"The 3D CFD model accounted for flow dynamics, eliminating the challenges of using 2D projected synchrotron X-ray images for velocity measurements."

References

[1] L. Aucott, H. Dong, W. Mirihanage, R. Atwood, A. Kidess, S. Gao, S. Wen, J. Marsden, S. Feng, M. Tong, T. Connolley, M. Drakopoulos, C.R. Kleijn, I.M. Richardson, D.J. Browne, R.H. Mathiesen, Helen. V Atkinson, Revealing internal flow behaviour in arc welding and

additive manufacturing of metals, Nat Commun 9 (2018) 5414. https://doi.org/10.1038/s41467-018-07900-9.

[2] Q. Guo, M. Qu, L.I. Escano, S.M.H. Hojjatzadeh, Z. Young, K. Fezzaa, L. Chen, Revealing melt flow instabilities in laser powder bed fusion additive manufacturing of aluminum alloy via in-situ high-speed X-ray imaging, Int J Mach Tools Manuf 175 (2022) 103861. https://doi.org/https://doi.org/10.1016/j.ijmachtools.2022.103861.

[3] S.M.H. Hojjatzadeh, N.D. Parab, W. Yan, Q. Guo, L. Xiong, C. Zhao, M. Qu, L.I. Escano, X. Xiao, K. Fezzaa, W. Everhart, T. Sun, L. Chen, Pore elimination mechanisms during 3D printing of metals, Nat Commun 10 (2019) 3088. https://doi.org/10.1038/s41467-019-10973-9.